Available online at www.sciencedirect.com
ScienceDirect
Geochimica et Cosmochimica Acta 73 (2009) 1487–1504
Geochimica et Cosmochimica Acta
www.elsevier.com/locate/gca

Experimental studies of metal–silicate partitioning of Sb: Implications for the terrestrial and lunar mantles

K. Righter [a,b,*], M. Humayun [c,d], A.J. Campbell [c,e], L. Danielson [a], D. Hill [b], M.J. Drake [b]

[a] Mailcode KT, NASA-JSC, 2101 NASA Parkway, Houston, TX 77058, USA
[b] Lunar and Planetary Laboratory, University of Arizona, Tucson, AZ 85721, USA
[c] Dept. of the Geophysical Sciences, University of Chicago, Chicago, IL 60637, USA
[d] National High Magnetic Field Laboratory, Florida State University, Tallahassee, FL 32310-3706, USA
[e] Dept. of Geology, University of Maryland, College Park, MD 20742, USA

Received 7 May 2008; accepted in revised form 25 November 2008; available online 16 December 2008

Abstract

The terrestrial mantle has a well defined Sb depletion of $\sim 7 \pm 1$ (Jochum and Hofmann, 1997), and the lunar mantle is depleted relative to the Earth by a factor of $\sim 50 \pm 5$ (Wolf and Anders, 1980). Despite these well defined depletions, there are few data upon which to evaluate their origin—whether due to volatility or core formation. We have carried out a series of experiments to isolate several variables such as oxygen fugacity, temperature, pressure, and silicate and metallic melt compositions, on the magnitude of $D_{Sb}^{met/sil}$. The activity of Sb in FeNi metal is strongly composition dependent such that solubility of Sb as a function of fO_2 must be corrected for the metal composition. When the correction is applied, Sb solubility is consistent with 3+ valence. Temperature series (at 1.5 GPa) shows that $D_{Sb}^{met/sil}$ decreases by a factor of 100 over 400 °C, and a pressure series exhibits an additional decrease between ambient pressure (100 MPa) and 13 GPa. A strong dependence upon silicate melt composition is evident from a factor of 100 decrease in $D_{Sb}^{met/sil}$ between nbo/t values of 0.3 and 1.7. Consideration of all these variables indicates that the small Sb depletion for the Earth's mantle can be explained by high PT equilibrium partitioning between metal and silicate melt $D_{Sb}^{met/sil}$. The relatively large lunar Sb depletion can also be explained by segregation of a small metallic core, at lower pressure conditions where $D_{Sb}^{met/sil}$ is much higher (2500).
Published by Elsevier Ltd.

1. INTRODUCTION

Siderophile elements provide clues to the conditions under which terrestrial planets and asteroids differentiated into core and mantle. Concentrations of these elements in mantles and basalts have formed the basis of models for Earth accretion, for example (Ringwood, 1979; Wänke, 1981; Jones and Drake, 1986). Recent models have proposed that the concentrations of the moderately siderophile elements (MSE; Ni, Co, Mo, W, P) in the terrestrial upper mantle have been set by metal–silicate equilibrium in an early magma ocean (Walter et al., 2000; Rubie et al., 2003). Other siderophile elements such as the highly siderophile (HSE; Re, Au and PGE) and chalcophile elements (Cu, Sn, Cd) are currently under evaluation for consistency with this model (e.g., Righter, 2005). Another class of elements, the volatile, siderophile elements includes Bi, Te, As and Sb. These elements can be depleted in planetary mantles (Fig. 1) by either volatility or core formation (or both), and figure into two aspects of the geochemistry of the Earth and Moon.

First, Sb has a very well-defined depletion in the Earth's primitive upper mantle (Jochum and Hofmann, 1997). Even

* Corresponding author. Address: Mailcode KT, NASA-JSC, 2101 NASA Parkway, Houston, TX 77058, USA. Fax: +1 281 483 5347.
E-mail address: kevin.righter-1@nasa.gov (K. Righter).

0016-7037/$ - see front matter Published by Elsevier Ltd.
doi:10.1016/j.gca.2008.11.042

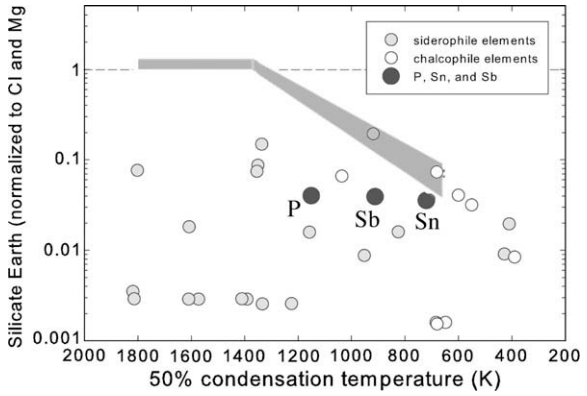

Fig. 1. Concentrations of siderophile elements in the terrestrial primitive upper mantle, relative to CI chondrites, plotted against 50% condensation temperature for the metal. Depletions of volatile siderophile elements are due in part to volatility, as shown by shaded region. Antimony, tin, and phosphorus plot below the volatility trend indicating that a further depletion is likely due to core formation. Condensation temperatures for elements are commonly tabulated in 50% values which indicates the temperature at which the element falls to 50% of its initial value in the gas (e.g., Wasson, 1985); the abundances of the volatile elements are thought be a reflection of condensation processes in the early solar nebula. Data are from McDonough and Sun (1995).

though there has been some uncertainty in the primitive mantle abundance of Sb due to fractionations between hydrothermal fluids, oceanic crust, continental crust and residual mantle (e.g., Sims et al., 1990; Noll et al., 1996), estimates of Sb in the primitive upper mantle have improved with new analyses and analytical approaches (Jochum and Hofmann, 1997; Schmidt et al., 2003; Fig. 2). Antimony has also been particularly difficult to explain in traditional models such as heterogeneous accretion. Because at low pressures $D_{Sb}^{met/sil}$ (where D is defined as the weight ratio of Sb in the metal/Sb in the silicate melt) is near 1200 (Newsom and Sims, 1991), heterogeneous accretion models predict a much larger depletion than is actually observed (also true for As). In addition, some have argued that volatile elements were added to the terrestrial upper mantle in a late accretion event, after the core segregated from the mantle (Yi et al., 1995, 2000). Second, the Moon's mantle is depleted in volatile elements relative to the Earth's mantle (Wolf and Anders, 1980), and a satisfactory explanation for this difference has yet to be advanced. One possibility is that the Moon's small core formed at lower pressure and reduced conditions relative to the Earth's core, and thus has a different depletion (Righter, 2002), but it is also possible that volatile elements were fundamentally different in the bulk Moon material after the high temperatures of the giant Moon-forming impact (Humayun and Clayton, 1995; Pahlevan and Stevenson, 2007; Righter, 2007).

Sophisticated models for Sb have not been proposed due to a dearth of experimental data and lack of understanding of its behavior at high pressures and temperatures. Determining the temperature and pressure dependences of $D_{Sb}^{met/sil}$ is required to determine if Sb abundances are consistent with high PT terrestrial magma ocean models (Li and Agee, 1996; Ohtani et al., 1997; Righter and Drake, 1999), and/or with conditions proposed for the segregation of the lunar core (e.g., Newsom, 1984; Righter, 2002). In order to address these fundamental questions about the Earth–Moon system, we have undertaken a study to understand the effects of oxygen fugacity, temperature, composition, and pressure on the partitioning of Sb between metal and silicate melt. Additional trace elements (Sn, Pd, P) were analyzed from some experimental charges. The experimental results will first be used to demonstrate a strong dependence of $D_{Sb}^{met/sil}$ on the Fe:Ni ratio of the metallic liquid, similar to that demonstrated for Ge and Sn (Capobianco et al., 1999). After demonstrating the effects of variable metal composition, fO_2, temperature, silicate melt composition

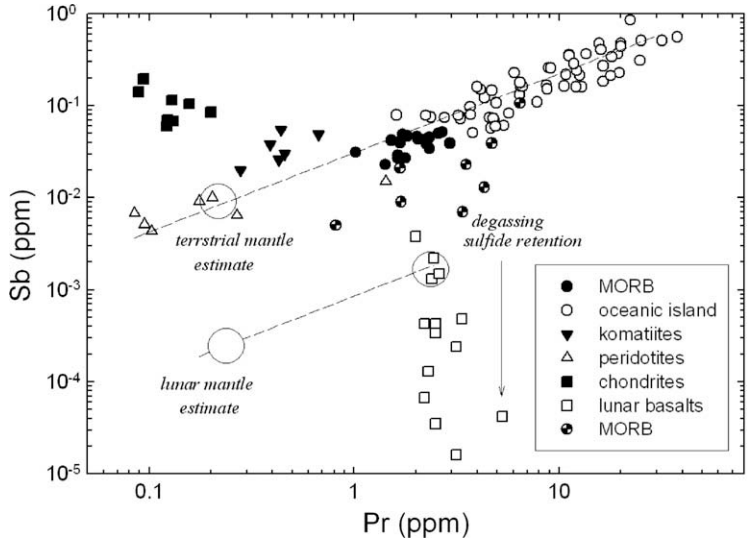

Fig. 2. Sb vs. Pr for ocean island basalt (OIB), mid-ocean ridge basalt (MORB), and mantle peridotite, defining an antimony depletion for the primitive upper mantle of the Earth (data from Morgan et al. (1978), Newsom et al. (1986), Sims et al. (1990), Jochum and Hofmann (1997), Schmidt et al. (2003)). Open square symbols are lunar basalts, which exhibit a much larger depletion in the lunar mantle compared to the terrestrial mantle (data from Wolf et al., 1979). Also shown are data for chondrites from compilation of Newsom (1995).

and pressure, applications of metal–silicate partition coefficients for Sb will be made to the Earth and Moon.

2. EXPERIMENTAL METHODS AND APPROACH

Experiments at 1 bar were done in Deltech vertical resistance furnaces at the University of Arizona. Alumina crucibles containing Sb-doped synthetic eucritic basalt and mixtures of Fe–Ni–S metal were sealed into evacuated silica tubes (see Capobianco et al., 1999). Variable Fe/Ni ratios in the metal phase controlled the oxygen fugacity through Fe–FeO equilibria (see below). The silica tubes were held in the hotspot of the furnaces for up to 7 days at 1260 °C and then quenched by rapid removal from the furnace. Minor reaction of the crucible with the silicate melt is evident from the presence of thin (10 μm) layer of (Fe, Mg)Al_2O_4 spinel at the crucible/melt interface (see also Capobianco et al., 1999).

Experiments at high pressures were conducted using both a non end-loaded piston cylinder apparatus, and a multi-anvil module in an 880 ton press. The piston cylinder has been calibrated for pressure using fayalite–ferrosilite equilibria and the melting point of diopside (Righter et al., 2006; Filiberto et al., 2007) requiring a correction of 0.03 GPa to the applied pressure; pressure and temperature are precise to ±0.05 GPa and ±5 °C, respectively. The multi-anvil assembly has been calibrated for pressure using SiO_2 transitions (at 9.4 GPa, 1600 °C), $(Mg_{82}Fe_{18})_2SiO_4$ transitions from olivine to wadsleyite (13.4 GPa, 1400 °C), and Mg_2SiO_4 transitions from wadsleyite to ringwoodite (15.0 GPa, 1200 °C, and 20.0 GPa, 1600 °C) using a 10/5 assembly with pre-cast octahedra, pyrophyllite gaskets, Re foil furnaces, and type C Re/W thermocouples (Leinenweber et al., 2006). Phases for calibration experiments were identified using Raman spectroscopy at NASA-JSC. Raman scattering measurements were made using a Jobin-Yvon Triax 550 spectrograph and a LabRAM HR high resolution Raman microscope. Scattering was excited by the 514.33 nm line of a coherent Ar^+ laser. The scattered radiation was collected through a long-working distance 50× objective. Pressure and temperature are precise to ±0.2 GPa and ±5 °C, respectively; temperature gradients are no larger than 50 °C, and thermocouple emf has not been corrected for pressure (see Righter et al., 2008a, for additional calibration details). Error bars on the three highest pressure runs are larger than 5 °C due to additional uncertainty introduced by controlling by power (based on a power curve for the 10/5 assembly).

Basalt powder doped with 1 wt.% Sb_2O_3, and for some experiments also Fe or FePd alloy, was encapsulated with either Fe metal (Fig. 3a), graphite (Fig. 3b) or MgO (Fig. 3c) (Table 1). Iron capsules react with the basalt starting material to produce slightly more FeO-rich liquids (Table 3). MgO capsules reacted with silicate melt at superliquidus conditions, to form more MgO-rich silicate melts (13–37 wt.% MgO; Fig. 4). Graphite capsules are less reactive with silicate melt (melt compositions are nearly constant, Table 3), but introduces C into the system (C in the metal and CO_2 in the silicate melt). All three capsule types were used in piston cylinder experiments, whereas

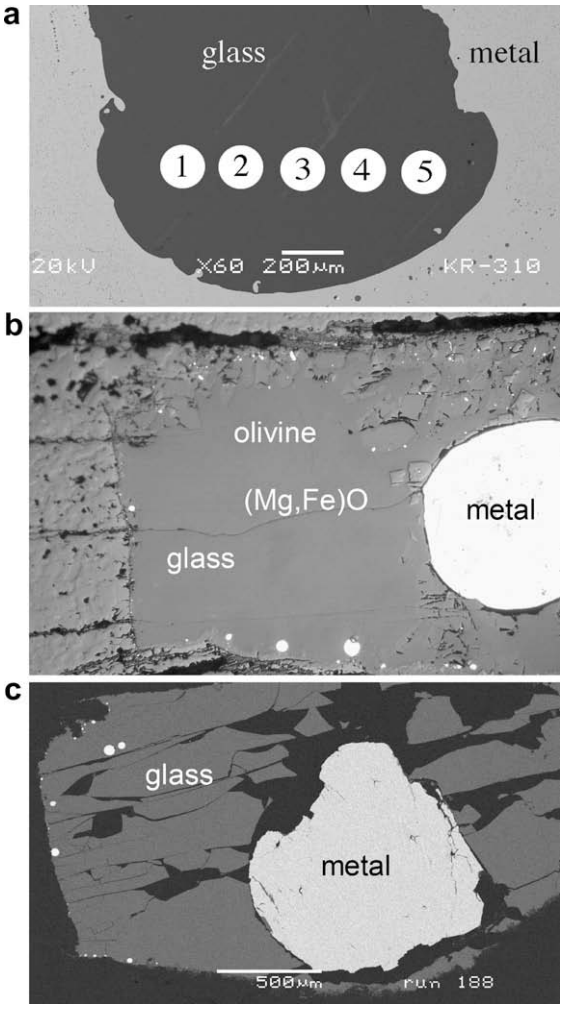

Fig. 3. Back scattered electron images of several different kinds of experimental run products. (a) Experiment #310 with Fe–Sb capsule, synthetic eucrite basaltic melt, and five different laser ablation pits, (b) experiment "MgO-3" with MgO capsule and basaltic melt at 1500 °C, 1.5 GPa; note equant (Mg, Fe)O and olivine crystals that also crystallized from the MgO enriched melt due to interaction with capsule (scale bar is the same as in figure c), and (c) experiment #188 with graphite capsule and basaltic silicate melt.

graphite (except Fe in #155) was used in the multi-anvil experiments (Table 1). Silicate samples with <20 wt.% MgO typically quench to glass (Fig. 3b), but those with >20 wt.% MgO contain a fine grained matte of silicate quench crystals. Similarly, the metallic liquid quenches to two phases—intergrown Fe–Pd–S–Sb alloy and sulfide.

Oxygen fugacity in 1 bar runs was controlled by variable Fe/Ni ratios of the metal (Capobianco et al., 1999). Oxygen fugacity in all runs was calculated using the activity of Fe in metal (using Swartzendruber et al., 1991; Pei et al., 1995; Voisin et al., 2003 for the FeNiSb system) and the activity of FeO in the glass (from Holzheid et al., 1997), and ranged from 2.5 logfO_2 units below to 1.5 logfO_2 units above the iron-wüstite buffer (Table 1). Oxygen fugacity for each experiment was calculated relative to the *IW* buffer, using

Table 1
Summary of experimental conditions and results (h, hours; m, minutes).

Run	P (GPa)	T (C)	Time	Capsule	Silicate	ΔIW	Phases	γSb	D(Sb)	High D/low D	γD(Sb)	D(Sn)	High/low D	D(P)	High/low D
JC1	0.0001	1260	72 h	Al_2O_3	Syn. Euc.	−1.06	sm, lm, ls	1.19	83800	95240/74600	99800	—		—	
JC2	0.0001	1260	72 h	Al_2O_3	Syn. Euc.	2.67	sm, lm, ls	0.060	270	315/230	230	—		—	
JC2 R3	0.0001	1260	72 h	Al_2O_3	Syn. Euc.	1.60	sm, lm, ls	0.070	334	380/300	340			—	—
						2.21		0.12	1300	1480/1170	150				
JC3	0.0001	1260	72 h	Al_2O_3	Syn. Euc.	0.25	sm, lm, ls	0.14	3620	4100/3240	6900	—		—	
JC3 R5A	0.0001	1260	72 h	Al_2O_3	Syn. Euc.	0.54	sm, lm, ls	0.19	*6700*	—	*1300*	—		—	
JC3 R4B	0.0001	1260	72 h	Al_2O_3	Syn. Euc.	1.15	sm, lm, ls	0.08	*500*	—	*600*	—		—	
JC4 R4B	0.0001	1260	72 h	Al_2O_3	Syn. Euc.	1.65	sm, lm, ls	0.13	*630*	—	*84*	—		—	
JC5 R4	0.0001	1260	72 h	Al_2O_3	Syn. Euc.	2.15	sm, lm, ls	0.13	3170	3540/2900	419	—		—	
Fe or FeNiCo capsule															
62	1.0	1300	4 h	FeNiCo	Syn. Euc.	1.65	sm, lm, ls	0.59	1430	1800/1100	12000	—	—	—	—
69	1.0	1250	4 h	FeNiCo	Syn. Euc.	2.15	sm, lm, ls	0.60	3480	3680/3100	29400	—	—	—	—
155	7.0	1800	1 h	Fe	Syn. Euc.	−0.99	lm, ls	1.96	3240	3720/2840	6300	—	—	—	—
160	1.0	1400	7 h	Fe	Syn. Euc.	−1.45	sm, ls	1.50	520	601/460	11000	—	—	—	—
165	1.0	1500	6 h	Fe	Syn. Euc.	−1.66	sm, ls	1.75	1860	2200/1560	46200	—	—	—	—
307	1.0	1500	10.5 h	Fe	eucrite	−1.25	sm, ls	1.73	9260	11000/7700	226000	—	—	—	—
309	1.0	1500	17 h	Fe	ank. + 10%	−2.14	sm, ls	1.75	58200	73600/45300	1450000	—	—	—	—
310	1.0	1500	4 h	Fe	ank.	−2.91	sm, ls	1.75	19600	24600/15700	489000	—	—	—	—
311	1.0	1500	3.5 h	Fe	DiAn	−3.41	sm, ls	1.76	1760	2500/1100	44300	—	—	—	—
312	1.0	1500	13 h	Fe	Di	−1.82	sm, ls	1.76	1700	2240/1230	42500	—	—	—	—
MgO capsule															
1	1.5	1700	40 m	MgO	ank. + Fe, FeS, Pd, Re	−1.89	lm, ls, ol	1.76	22	26/19	48	—		—	
2	1.5	1700	30 m	MgO	basalt + Fe, FeS, Pd, Re	−2.01	lm, ls, ol	2.17	711	815/625	1470	—		2.71	3.5/2.3
3	1.5	1500	4.3 h	MgO	basalt + Fe, FeS, Pd	−2.12	lm, ls, ol	2.07	818	950/710	1280	14.8	20.6/11.1	10.0	13.3/8.0
4	1.5	1700	45 m	MgO	basalt + Fe, FeS, Pd	−2.34	lm, ls, ol	1.56	376	430/330	760	9.3	12.3/7.3	—	
5	1.5	1600	2 h	MgO	basalt + Fe, FeS, Pd	−2.26	lm, ls, ol	2.01	4200	4800/3700	7700	—		4.1	5.8/3.3
6	1.5	1600	1 h	MgO	rhyolite + Fe, FeS, Pd	−2.77	lm, ls, px	1.82	209	245/180	410	6.6	7.4/5.8	22.7	30/16
8	1.5	1800	10 m	MgO	basalt + Fe, FeS, Pd	−2.27	lm, ls	1.95	933	1100/790	2230	6.7	8.1/5.7	1.57	2.4/1.1
9	1.5	1600	1 h	MgO	Andesite + Fe, FeS, Pd	−2.47	lm, ls	2.39	1105	1270/970	2030	—	—	25.4	30.0/21.7
12	1.5	1900	10 h	MgO	basalt, $Fe_{95}Pd_5$	−2.40	lm, ls	1.84	2304	2600/2100	5370	—	—	5.6	7.2/4.3
14	1.5	1800	10 h	MgO	basalt, $Fe_{50}Pd_{50}$	−2.24	lm, ls	2.33	371	420/330	615	16	18.5/13.3	3.5	4.2/2.9
C capsule															
7	1.5	1600	1 h	C	basalt, $Fe_{95}Pd_5$	−1.95	lm, ls, px	1.90	119	144/98	179	8.4	0.82	—	—
10	1.5	1400	8 h	C	basalt, $Fe_{95}Pd_5$	−2.01	lm, ls	1.47	5790	8730/4320	7573	80.1	—	—	—
11	1.5	1800	12 m	C	basalt, $Fe_{95}Pd_5$	−1.99	lm, ls	2.36	15	18/12	25	21	0.5	—	—
15	1.5	1800	15 m	C	basalt, $Fe_{50}Pd_{50}$	−1.73	lm, ls	1.95	97	115/83	145	75	7.2	—	—
High pressure															
59	12.0	1900	1.5 m	C	basalt, $Fe_{50}Pd_{50}$	−1.97	lm, ls	1.98	6	8/5.4	13	100	120/84	<0.19	—
62	13.0	2100	3 m	C	basalt, $Fe_{50}Pd_{50}$	−2.00	lm, ls	2.38	0.42	0.6/0.3	1	—	—	<0.23	—
63	15.0	2150	3 m	C	basalt, $Fe_{50}Pd_{50}$	0.34	lm, ls	1.02	209	240/185	213	27	34/22	<0.15	—

Experiments 1–5 had the following measured/calculated olivine contents (Fo%). (1) 92/93, (2) 94/94, (3) 88/89, (4) 96/97, (5) 93/94 (see text for details).
Italicized values are not used in the modeling since Sb contents are suspect (see text for Section 5).

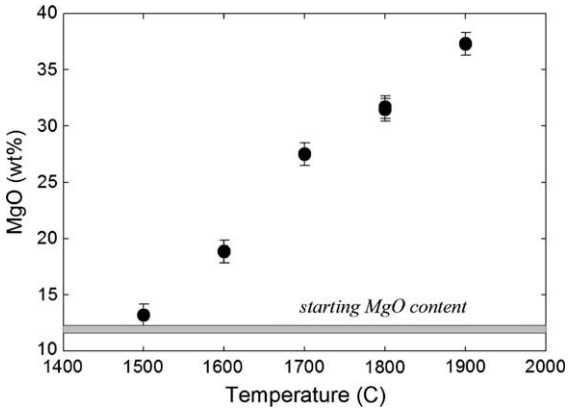

Fig. 4. Correlation between temperature and MgO content of silicate melt in experiments with basalt and MgO capsules (experiments 3–5, 8, 12, 14). Correlation is due to temperature dependence of reaction between capsule and basalt. Horizontal shaded line represents the MgO content of the starting material.

the relation $\Delta IW = -2^{*}\log(a_{Fe}/a_{FeO})$, where oxygen fugacity for the *IW* buffer at *P* and *T* was calculated using the expression of Righter et al. (1997). At the higher oxygen fugacities of the 1 bar experiments, some of the oxidized iron can be present as Fe_2O_3 as well as FeO. The amount of Fe_2O_3 can be estimated using the calibration of Kress and Carmichael (1991) where FeO and Fe_2O_3 can be calculated knowing temperature, fO_2, and melt composition. For these experiments, the amount of calculated $XFe_2O_3/XFeO$ varies from 0.069 in the most oxidized runs (JC2R3) to 0.013 in the most reduced runs (JC2). The amount of Fe_2O_3 is thus small, but we nonetheless acknowledge its presence. This small amount of Fe_2O_3 will not have a significant effect on silicate melt structural characteristics such as nbo/t values (used in later assessments). For example, nbo/t calculated using all FeO compared to the calculated FeO and Fe_2O_3 are 0.82 and 0.79, respectively, for the glass with the most Fe_2O_3 (JC3R5A). In addition, for this same glass, nbo/t changes from 0.79 to 0.84, when assuming that Fe_2O_3 is in IV or VI tetrahedral coordination, respectively, calculated as outlined by Mills (1993).

The techniques described above were utilized in several different series designed to isolate the effect of specific variables. First, the 1 bar runs (JC series) were designed to evaluate the effect of variable metal Fe/Ni ratio on the magnitude of $D_{Sb}^{met/sil}$ under low pressure conditions, and to study the valence of Sb as a function of fO_2, as was previously done by Capobianco et al. (1999) for Ga and Sn. Second, the experiments in graphite capsules, and fixed pressure and silicate melt composition, were used to evaluate the effect of temperature (runs 7, 10, 11 and 15). Third, the effect of melt composition was evaluated at 1500 °C using the range of melt compositions in the 300 series runs, and after making corrections (see below) for valence and temperature from the previous two series. And finally, the effect of pressure was evaluated in experiments between 100 MPa and 13 GPa, with corrections (see below) due to variable fO_2, T and melt composition applied to the last series of experiments.

3. ANALYTICAL TECHNIQUES

3.1. Electron microprobe analysis (EMPA)

Quenched run products were mounted in epoxy, cut and polished and analyzed with an electron microprobe for major elements with a CAMECA SX100 electron microprobe, using an accelerating voltage of 20 kV and sample current of 20 to 40 nA. Multiphase quenched silicate melt and metallic melt were analyzed by rastering the beam over 10×10 μm area. Standards include both natural (kaersutite, wollastonite, chromite, rutile, olivine, rhodonite, potassium feldspar, albite) and synthetic (Sb, Pd, Re and Sn metals, NiO) standard materials. Counting times for major elements was typically 10 s, and as long as 120 s for low concentrations of Ni or Cr in silicates. Under the latter conditions, detection limits were approximately 100 ppm. PAP $\varphi-\rho-Z$ corrections were used in the data reduction (Pouchou and Pichoir, 1991). Typical uncertainty for major elements analyzed by the NASA-JSC electron microprobe is <2%, and for Sb and *P* in metals <5%. Carbon contents of metals were analyzed using a set of C-bearing steel standards with C contents between 0.08 and 2.78 wt.% C (BCS 152/3, 402 and 234/8 and LECO 501–504 and 501–505). Analysis was done with a PC2 crystal in differential mode counting for 20 s, and samples were not carbon coated, but instead a strip of carbon tape was used from holder frame to the metal sample edge.

3.2. Instrumental neutron activation analysis (INAA)

Glass cores (0.16–0.95 mg) were extracted from doubly polished thin sections of the JC run products using a microdrill. They were packaged in pre-cleaned, high purity polyethylene vials and then transferred to new containers after irradiation (see Hill et al., 1991; Swindle et al., 1998). The glasses were irradiated at the University of Arizona Nuclear Reactor Laboratory's TRIGA reactor with neutron fluence of 7.1×10^{15} ncm^{-2} (lazy susan). The samples and standards were assayed on the fast-timing anticoincidence/coincidence, Compton suppression system consisting of a PGT coaxial GeLi detector/NaI scintillator, 58.4 mm diameter, 36.5 mm length with 24% efficiency. This anti-Compton system greatly reduces the continuum from scattered X-rays and allows a greater sensitivity for most elements such as antimony (Boynton and Hill, 1983). Standards included a set of synthetic mixtures along with NIST SRM 1633a Coal Fly Ash, Allende USNM 3529 sp13 pos22, and CRB (<100 mesh made by Dale Hill split 9/2/75 B.C.). The assay periods were typically: 6 h–4 days; 4 days–2 weeks; 4–8 weeks after end of bombardment (EOB). Counting times ranged from 2 to 12 h each with one to four counts per assay period. Because ^{122}Sb was the most useful radionuclide ($t½ = 64$ h), the earlier counts were the most relevant for this study.

3.3. Laser ablation inductively coupled plasma mass spectrometry (LA-ICP-MS)

For trace element analyses, a Finnegan Element™ magnetic sector ICP-MS was used at both University of

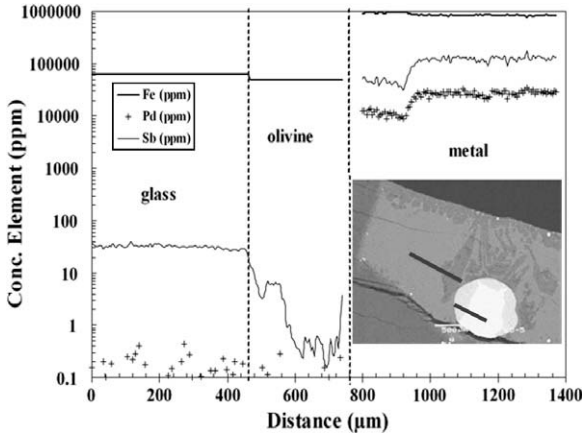

Fig. 5. Profile from laser ablation analyses in run #5, which includes glass, olivine and metal. There were detectable amounts of Sb and Sn in the glass, but Ru, Pd, and Re were too low in the glass despite their measurable concentrations in the metal. There is a patch of glass that interferes with the left hand side of the olivine analysis, and so only the right hand side of the analysis track through olivine is used for the Sb concentration in olivine.

Chicago and Florida State University (FSU). The former lab used a CETAC Transgenomics LSX-200 (266 nm) UV laser system, whereas the latter used a New Wave UP213 (213 nm) laser system. At Chicago, ^{57}Fe, ^{121}Sb, ^{69}Ga and ^{75}As were analyzed (for runs 307–312), whereas at FSU, the peaks ^{25}Mg, ^{57}Fe, ^{59}Co, ^{60}Ni, ^{102}Ru, ^{105}Pd, ^{106}Pd, ^{120}Sn, ^{121}Sb, and ^{123}Sb were monitored in low resolution mode at 50 ms/peak (for runs 1–63). Silicate glasses were analyzed with an 80 μm diameter track scanned at 10 μm/s, and quenched metallic liquids were analyzed with 12–15 μm diameter tracks scanned at 5 μm/s, using 10 Hz laser repetition rate and 50% power output. The NIST SRM 1263a steel, and iron meteorites North Chile (Filomena) and Hoba were used as standards, as described in greater detail by Campbell and Humayun (1999) and Campbell et al. (2002). The advantage to this approach is that one can analyze several phases in a single traverse (Fig. 5) and select areas that may have been affected by metal or other phases not visible in the polished mount because they are below the surface. Typical uncertainty for trace elements analyzed by LA-ICP-MS is <10% (Humayun et al., 2007).

4. RESULTS

4.1. Concentrations of Sb, Sn, C and P in metals and silicate melts

Concentrations of Sb in the 1 bar experimental glasses ranged from 25 to 430 ppm, corresponding to $D_{Sb}^{met/sil}$ of 416–17200. In comparison, the Sb concentrations in silicates from the high pressure and temperature experiments ranged from 1 to 1360 ppm, with $D_{Sb}^{met/sil}$ from 6 to 83800 (Tables 2 and 3). Tin concentrations in metal and silicate have also been determined by LA-ICP-MS, and are all <220 ppm (Table 3). The values of $D_{Sn}^{met/sil}$ range from 6.6 to 100 for 11 different experiments. Phosphorus is detectable in some silicates and metals, present up to 0.28 wt.% P_2O_5 and up to 1.22 wt.% P, respectively. Values for $D_{P}^{met/sil}$ range from 1.57 to 25.4 from eight different experiments, with three other experiments only providing an upper limit (Table 1). These new values for $D_{Sn}^{met/sil}$ and $D_{P}^{met/sil}$ will be integrated with previous results for Sn and P in the discussion Section 5.2. Finally, palladium concentrations in the metal (<4 wt.% and homogeneous profiles; Table 3) and silicate are reported in a separate paper focusing on Pd, and not discussed in detail here (Righter et al., 2008a). The error on the microprobe analyses of Sb and Sn in metal (5%), combined with the laser ablation analyses of Sb and Sn in glasses (~10%), results in uncertainties in the partition coefficients of approximately 15% (slightly lower for P–10%—because of smaller error on EMPA analyses for P).

Several of the JC series experimental glasses were analyzed using both micro-coring-INAA and LA-ICP-MS because the glassy regions are large enough in these experiments to use both techniques. Comparison of INAA and LA-ICP-MS results for Sb shows that the Sb concentrations obtained by LA-ICP-MS are lower (Table 3). The LA-ICP-MS results are preferred in this study because of the ability to remove or filter analyses that are affected by the interference of tiny Sb-rich metallic flakes. There are large Sb "spikes" of 10,000 cps in some of the laser ablation analyses that otherwise have a signal of ~1000 cps in the time resolved spectrum for ^{121}Sb and ^{123}Sb. These can be filtered out of the analysis because they are clearly due to an interfering metal flake. For example, analyses of JC1 by INAA yield 25 ppm Sb, compared to 4.85 ppm Sb by LA-ICP-MS. If the metal spike is not filtered out of the LA-ICP-MS analysis, the result is a concentration closer to that obtained by INAA, ~9 ppm. Because the INAA is sampling a larger sample volume and more vulnerable to the inclusion of even a small particle, we use the laser ablation results for all experiments. This is a similar situation to that for analysis of W and Re in previous experimental studies (Ertel et al., 2001; O'Neill et al., 2008), where bulk glass analyses yield higher siderophile element concentrations than laser ablation analyses, presumably due to the interference of included metal particles in the bulk analysis. The metallic flakes in question here should not confused with the micro-nugget flakes sometimes found in studies of highly siderophile elements such as Pt, or in cases where the activity of a siderophile element is high (see next section for an example for Sb).

Carbon contents measured in C-bearing metallic liquids ranged from 1.3 to 6.5 wt.% C, and can be compared to C contents calculated using Fe–C phase diagrams of Gustafson (1985) and Sundman et al. (1985). In all cases, the C content measured is lower than the calculated value, indicating that the phase diagram is really just a rough guide to C contents in a compositional system that also has Pd, Sb, and Re. All microprobe analyses are reported in Tables 2 and 3.

4.2. Nugget problem

A small number of runs (302, 303, 306, 308, 300, but not reported in the tables) were not possible to use in this

Table 2
Electron microprobe and LA-ICP-MS analyses of metals (s) and metallic liquids (l).

Run		Fe	Ni	Sb	S	P	C[b]	Pd	Re	Sn[a]	Total
JC1	l	60	—	39.4(6)	—	—	—	—	—	—	99.40
JC2	s	1.54	96.25	1.03(8)	—	—	—	—	—	—	98.82
JC2 R3	l	0.76	74.38	24.39(12)	—	—	—	—	—	—	99.54
JC2 R3	s	1.71	91.27	6.25(8)	—	—	—	—	—	—	99.23
JC3	s	17.97	74.87	4.49(8)	—	—	—	—	—	—	97.33
JC3 R5A	l	11.28	56.40	31.45(13)	—	—	—	—	—	—	99.14
JC3 R4B	l	2.74	68.89	27.02(11)	—	—	—	—	—	—	99.65
JC4 R4B	s	6.36	86.20	5.88(9)	—	—	—	—	—	—	98.43
JC5 R4	l	1.15	69.67	27.34(14)	—	—	—	—	—	—	98.16
62[a]	l	30.53	29.57	3.48 (1.54)	25.06(3.97)	—	—	—	—	0.75(36)	98.98
69[a]	l	45.79	21.72	4.33 (3.23)	15.36(7.37)	—	—	—	—	0.71(8)	94.90
155	l	77.75	0.05	20.74(85)	—	—	—	—	—	—	98.55
160	s	96.5	0.15	2.15(8)	—	—	—	—	—	—	98.80
165	s	98.85	0.086	0.56(6)	—	—	—	—	—	—	99.49
307	s	97.78	0.49	1.25(12)	—	—	—	—	—	—	99.53
309	s	98.84	0.15	0.46(7)	—	—	—	—	—	—	99.44
310	s	99.29	0.10	0.55(8)	—	—	—	—	—	—	99.95
311	s	99.56	0.05	0.06(2)	—	—	—	—	—	—	99.67
312	s	99.21	0.08	0.18(4)	—	—	—	—	—	—	99.48
1	l	97.27	—	1.01(5)	1.533	—	—		0.066	—	99.88
2	l	88.41	—	6.19(25)	1.09	0.26	—	0.02	3.74(28)	—	99.71
3	l	90.05	—	2.29(9)	5.07	0.22	—	3.24(20)	0.03(1)	6.5(5)	100.90
4	l	91.1	—	5.0(2)	2.40	—	—	1.25(15)	0.06(1)	4.0(3)	99.81
5	l	84.9	—	10.7(3)	1.81	0.43	—	2.3(3)	—	8.3(7)	100.14
6	l	93.8	—	3.3(2)	0.13	0.10	—	1.4(2)	—	22.2(8)	98.73
8	l	90.3	—	2.8(2)	3.14	0.11	—	3.3(3)	—	4.0(3)	99.65
9	l	82.6	—	6.3(3)	2.75	1.22	—	5.4(4)	—	17(2)	99.27
12	l	87.91	—	6.52(8)	2.56	0.18	—	1.50(15)	—	—	98.67
14	l	59.12	—	4.82(5)	0.05	0.20	—	34.2(1.5)	0.09(1)	6.9(5)	98.28
7	l	85.3	—	0.64(5)	0.02	0.09	4.5 [4.8]	6.84(30)	—	4.2(3)	97.39
10	l	88.3	—	5.21(3)	0.07	—	4.3 [4.0]	2.0(2)	—	3.0(3)	99.88
11	l	88.25	—	0.24(2)	0.03	0.06	4.5 [5.5]	7.56(20)	—	19(2)	100.64
15	l	71.82	—	0.74(4)	0.14	0.56	3.9 [5.5]	24.15(30)	—	46.5(4.0)	101.31
59	l	47.2	—	0.38(3)	—	n.d.	2.8 [5.8]	18.9(1.2)	27.1(1.1)	220(18)	99.38
62	l	41.48	—	0.03(1)	0.07	n.d.	4.9 [6.4]	14.32(80)	37.04(2.1)	—	99.34
63	l	4.57	—	28.58(56)	0.12	n.d.	6.5 [6.5]	57.03(1.50)	1.86(34)	23(3)	98.66

Uncertainties for major elements by EMPA are <2% (Fe, Ni, S), and 10% for C.
[a] In ppm, except for 62 and 69 in wt.%; also 62 and 69 are from Righter and Drake (2000) and include other elements not reported in this table.
[b] Number in brackets is carbon calculated from the Fe–C phase diagram of Sundman et al. (1985).

study due to the presence of many finely dispersed FeSb particles in the glass (Fig. 6). The particles are present in such great abundance that they interfere with the analysis of the glasses by all techniques available—LA-ICP-MS, micro-coring and INAA, and EMPA. This situation is not unlike the nugget problem that affects the analysis of highly siderophile elements (e.g., Walter et al., 2000; Ertel et al., 2008), except that the small blebs are FeSb rich. Their presence is most likely due to the use of Sb metal as the source of Sb in these experiments starting materials. In subsequent experiments Sb_2O_3 was used (and at lower doping levels) and the metallic flakes were not observed. The metallic particles were not observed in any other runs and are specific to Fe capsules, Sb dopants and more evolved (silica rich) melt compositions. Mention is made here due to the potential relevance to nugget formation in general.

4.3. Equilibrium

Several experiments (MgO-1 to -5 using MgO capsules) crystallized olivine during the experiment, and the composition of the olivine and coexisting melt can be used to assess whether equilibrium was approached in the experiments. Olivine-melt K_d are consistent with equilibrium—calculated Fo contents (X_{Fo}) based on a comprehensive olivine-melt K_d(Mg–Fe) model of Toplis (2005) are within 0.01 of the measured olivine composition for each run (Table 1). Also, if the reaction of metal with silicate did not reach completion or equilibrium, there will be variable silicate compositions according to the equilibrium $2Fe + Mg_2SiO_4 + O_2 = 2MgO + Fe_2SiO_4$ and one might expect to find zoned metal or olivine. However, the olivines (or pyroxenes, where present) are not compositionally zoned, indicating that equilibrium has been attained (see

Table 3
Electron microprobe and LA-ICP-MS (for Sb and Sn) analyses of silicate phases (number for Sb in brackets are INAA measurements).

Run	SiO_2	TiO_2	Al_2O_3	Fe_2O_3	FeO	MnO	MgO	CaO	Na_2O	K_2O	P_2O_5	NiO	S	Total	Sb	Sn	[c]nbo/t
JC1	42.0	—	20.1	0.60	23.50	—	3.5	9.12	—	—	—	—	—	98.77	4.7(5) [25]	—	0.55
JC2	48.3	—	18.8	0.23	12.02	—	5.5	9.95	—	—	—	2.69	—	97.51	38.1(2.8) [48]	—	0.51
JC2 R3	48.9	—	19.4	1.21	11.86	—	5.6	10.01	—	—	—	2.47	—	99.41	187(21) [351]	—	0.51
JC3	38.9	—	19.6	1.21	26.33	—	3.0	8.43	—	—	—	0.20	—	97.72	12.4(1.2) [37]	—	0.80
JC3 R5A	39.4	—	19.6	1.61	26.61	—	3.3	8.47	—	—	—	0.08	—	99.11	–[47]	—	0.83
JC3 R4B	38.9	—	19.6	0.67	26.82	—	3.0	8.43	—	—	—	0.20	—	97.67	–[118]	—	0.83
JC4 R4B	42.1	—	19.9	0.72	23.34	—	3.5	8.90	—	—	—	0.84	—	99.31	–[428]	—	0.71
JC5 R4	43.9	—	19.1	0.80	17.73	—	4.3	9.05	—	—	—	1.54	—	96.36	86.3(8.8) [180]	—	0.61
				Cr_2O_3													
62	28.2		9.7		51.30		3.2	5.48						98.90	2.1(2)		2.42
69	39.0	1.54	11.8		34.17		3.3	5.45	2.67	1.25	0.20	—	0.30	99.37	2.1(2)		1.32
155	37.4		20.7	—	27.80	—	3.0	8.82	—	—	—	—	—	97.63	64(6)	—	0.81
160	47.2	0.05	21.4	0.08	19.51	0.37	3.2	6.14	0.07	0.03	—		—	97.97	41.1(4.0)	—	0.42
165	48.2	0.01	24.9		15.17		2.7	5.69	0.06	0.02	0.02		—	97.39	3.0(2)	—	0.21
307	41.3	0.01	18.0	0.26	25.02	1.53	4.3	7.67					—	98.09	1.35(11)	—	0.79
309	45.4	3.07	12.8	0.21	9.86	1.11	11.1	11.62	3.04	0.91	0.02	—	—	99.17	0.079(7)	—	0.95
310	44.8	3.14	12.7	0.30	4.17	2.73	16.5	10.80	2.68	1.01	0.01	—	—	98.84	0.28(3)	—	1.04
311	51.6	0.01	3.6	0.01	2.48	2.93	14.8	23.63					—	99.06	0.34(2)	—	1.70
312	44.7	0.01	10.5	0.45	13.93	6.93	8.0	13.82					—	98.32	1.06(8)	—	1.13
1	31.7	3.39	11.8	0.02	12.89	0.17	17.3	14.72	3.60	1.37	0.26	—	0.085	97.36	452(40)	—	2.27
oliv	39.3	0.12	0.43	—	7.68	0.11	49.2	0.95	0.03	—	0.05	—	—	97.88	—	—	—
2	34.5	1.31	14.4		11.13	0.28	22.4	9.49	2.86	0.36	0.22	—	0.06	97.04	87(8)	—	1.80
oliv	39.9	0.06	0.58		5.96	0.15	49.8	0.51	0.04	—	0.05	—	—	97.03	—	—	—
3	44.2	1.51	15.5	0.02	8.93	0.13	13.2	11.11	3.11	0.45	0.05	—	0.066	98.24	28(3)	0.44(10)	1.12
oliv	39.0	0.04	0.21	—	11.23	0.13	47.5	0.39	0.03	—	0.02	—	—	98.55	—	—	—
4	34.8	1.31	13.7	—	7.80	0.13	27.5	9.20	2.64	0.37	0.26	—	0.085	97.89	133(12)	0.43(8)	2.01
oliv	40.8	0.08	0.79	—	4.33	0.07	51.7	0.46	0.03	—	0.05	—	—	98.25	—	—	—
5	39.3	1.54	16.2	—	8.35	0.13	18.8	10.96	3.49	0.40	0.24	—	0.05	99.51	25.4(2.5)	—	1.37
quench	38.5	1.47	15.5	—	7.88	0.14	19.2	10.66	3.20	0.40	0.22	—	0.05	97.17	—	—	1.37
oliv	39.7	0.05	0.50	—	6.20	0.09	49.7	0.39	0.03	—	0.04	—	—	97.31	0.41(4)	—	—
6	55.5	0.06	12.3	0.01	4.85	0.09	18.3	1.08	3.90	2.66	0.01	n.a.	0.02	98.82	158(15)	3.4(3)	0.88
6 pyroxene	57.9	0.03	2.6	n.d.	3.39	0.06	36.1	0.15	0.10	n.d.	n.d.	n.a.	—	100.41	28(3)	—	—
8	32.0	1.26	14.0	—	9.17	0.11	31.5	8.61	2.77	0.34	0.16	—	0.20	100.5	30(3)	0.59(6)	2.36
9	48.0	0.58	15.9	0.01	6.54	0.08	18.3	5.02	3.42	1.51	0.11	—	0.042	99.45	57(5)	—	0.99
12	32.1	0.91	10.8	0.03	7.65	0.09	37.3	6.99	2.10	0.29	0.074	—	0.21	98.54	28.3(2.5)	—	2.46
14	35.1	1.27	12.3	0.02	7.27	0.12	31.7	9.13	2.48	0.38	0.13	—	0.025	99.91	130(14)	0.44(4)	2.38
7 (188)	46.7	1.44	16.7	—	11.32	0.15	8.6	9.54	3.10	0.36	0.25	—	—	98.16	54(6)	0.5(1)	0.77
pyx	58.0	0.04	2.45	—	3.34	0.07	36.3	0.14	0.07	—	—	—	—	100.38		—	—
10	48.3	1.42	16.9	—	10.76	—	8.5	9.56	2.93	0.34	0.27	—	—	98.92	9(3)	0.04(1)	0.72
11	47.8	1.41	16.5	—	10.74	—	8.4	9.33	3.05	0.36	0.28	—	—	97.9	161(15)	0.90(8)	0.73
15	47.1	1.32	17.0	—	13.07	—	8.4	9.51	3.18	0.34	0.18	—	—	100.07	76(8)	0.60(6)	0.79
59	47.2	1.19	17.8	—	9.16	—	9.0	9.68	3.37	0.21	0.12	—	—	97.63	591(60)	2.2(2)	0.77
62	47.2	1.13	18.2	—	9.36	—	8.7	9.87	3.21	0.22	0.10	—	—	97.89	712(70)	—	0.73
63	48.1	1.56	17.7	—	9.32	—	8.6	9.66	3.11	0.29	0.15	—	—	98.45	1370(140)	0.85(8)	0.74

Uncertainties for major elements by EMPA are <2%.
[c] nbo/t calculated as defined by Mills (1993) and taking into account the presence of Fe_2O_3 in the more oxidized runs (JC series at 1 bar).

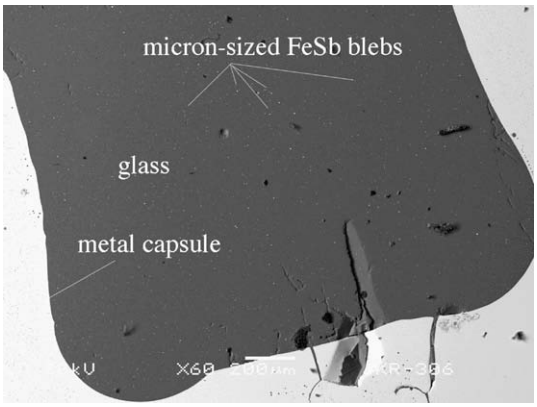

Fig. 6. Back scattered electron (BSE) image for experiment #306, illustrating the nugget problem. Dispersed throughout the glass are micron-sized FeSb blebs that interfere with the analysis of the glass. Scale bar is 200 μm. Capsule is Fe metal.

Table 1). Another approach to evaluating equilibrium in high temperature experiments is to consider scales required for diffusion rates of various cations in the silicate system. Diffusion coefficients for Sc and Sb, both 3+ valence, in silicate melts at 1400 °C, are $\sim 10^{-6}$ (LaTourrette et al., 1996; Claussen et al., 1999) which corresponds to a timeframe of ~10 h. for equilibration across a 2 mm distance. Using diffusion data of Claussen et al. (1999) it can be shown that all of our experimental run durations are longer than required to satisfy the diffusion distance within the capsules. This is ample time for equilibrium, especially since the simple calculation does not take into account convective transport which will be much faster. Finally, the experiments reported here are longer than experiments for which time series have been done for even slower diffusing elements such as W^{4+} and P^{5+}, as well and Ga^{3+} and Sn^{4+} (Righter et al., 1997; Righter and Drake, 1999, 2000).

4.4. Systematics of metal–silicate partition coefficients for Sb

4.4.1. Corrections for solid metal/liquid metal

Several lower temperature experiments (300 series, 160 and 165) contain solid metal instead of liquid metal. A liquid metal will have a different affinity than a solid metal for a trace element such as Sb, even in S- and C-free metallic systems. Several recent studies have determined the partitioning of Sb between solid and liquid metal, and when the metallic liquid system is S-free and C-free, $D_{Sb}^{solid-metal/liquid-metal} = 0.06$ (Chabot et al., 2003, 2006, in press). For this reason, we have corrected the 300 series, and 160 and 165 (Table 1) by dividing $D_{Sb}^{solid-metal/liquid-sil}$ by $D_{Sb}^{solid-metal/liquid-metal}$ and thus yielding $D_{Sb}^{liquid-metal/liquid-sil}$ so that they can be directly compared to other liquid metal partitioning results $D_{Sb}^{met/sil}$ in this study.

4.4.2. Metallic melt composition and oxygen fugacity—1 bar series

Usually, the slope of $\log D$ vs. $\log fO_2$ is related to the valence of an element dissolved in the silicate melt (e.g., Holzheid et al., 1997). However, for some elements (Ga, Ge, Sn; Capobianco et al., 1999), $\log D$–$\log fO_2$ diagrams yield slopes that indicate anomalously low valences, due to changes in activity coefficient with metal composition. Specifically, the value of the activity coefficient can change by up to several orders of magnitude with variable metal composition (or Fe/Ni ratio in the case of natural planetary systems). This is seen in some slag systems: Takeda et al. (1983) showed that although $D_{Sb}^{met/sil}$ is roughly correlated with a slope of Sb^{3+} there are deviations at lower fO_2, where the metal composition has changed. Yazawa (1980) showed an even greater deviation with distribution coefficients flattening out or even turning over at $\log fO_2 < -9$ at 1300 °C. Both of these studies were completed on Cu-rich and calcium or copper ferrite slags, so again the applicability to natural systems is uncertain.

For systems appropriate for cosmochemistry, the Fe/Ni ratio is most important. Differences in the topology of the Fe–X and Ni–X binaries can in turn affect the thermodynamics of the ternary system; systems with more intermetallic compounds are likely to have activity coefficients close to unity for the end members (Pei et al., 1995; Okamoto, 1999; Gupta, 2000; Raghavan, 2004). In the case of Sb, there are significant differences between the Fe–Sb and Ni–Sb binaries and, as predicted by Capobianco et al. (1999), the solubility of Sb levels out at lower oxygen fugacities, suggesting a valence change (Fig. 7). However, when activity-composition relations in the Fe–Ni–Sb system are considered, it becomes clear that there is no valence change, just a small activity correction that must be made for the metals. In this case, the activity coefficient of Sb in the Fe-NiSb system can be calculated according to:

$$RT \ln \gamma Sb = 2[X_{Sb}X_{Fe}W_{FeSb} + X_{Sb}X_{Ni}W_{NiSb}] + X_{Fe}2W_{SbFe} + X_{Ni}2W_{SbNi} + X_{Fe}X_{Ni}C_{FeNiSb} - 2Gxs$$

where

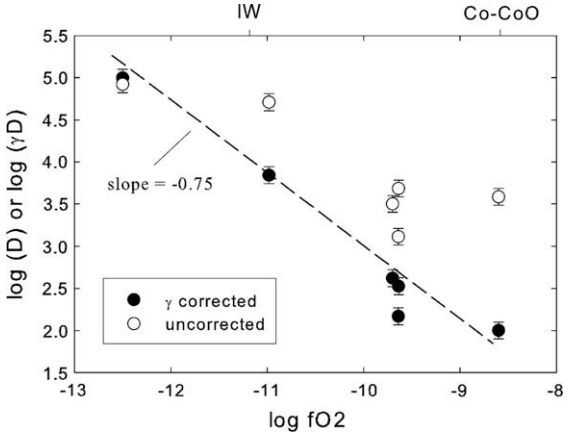

Fig. 7. Comparison of partition coefficient values, $D_{Sb}^{met/sil}$ (open circles), to those corrected for activity changes in the metal, γD (Sb) (solid circles). γ(Sb) is calculated using the expression derived in the text. Note the lower slope and the scatter at any given fO_2 in the uncorrected runs; activity corrections result in less scatter and also a slope of −0.75 which is expected for a 3+ valence for Sb. All experiments were carried out at 1260 °C, and include the JC series of Table 1.

$$Gxs = X_{Fe}X_{Ni}[W_{FeNi}X_{Fe} + W_{NiFe}X_{Ni}] + X_{Fe}X_{Sb}[W_{FeSb}X_{Fe} + W_{SbFe}X_{Sb}] + X_{Ni}X_{Sb}[W_{NiSb}X_{Sb} + W_{SbNi}X_{Sb}]$$

Margulies parameters (W) and constants (C_{FeNiSb}) are from Swartzendruber et al. (1991), Pei et al. (1995), Voisin et al. (2005), and the activity expression is for an asymmetric solution model from Mukhopadhyay et al. (1993) (some conversion of Redlich–Kister coefficients to Margulies parameters are required, after Cheng and Ganguly, 1994). The activity coefficient changes by several orders of magnitude over the range of Fe–Ni in the experiments (Fig. 8). When an activity coefficient correction is made ($\log \gamma D$ instead of $\log D$, as Capobianco et al., 1999, did for Ga, Ge and Sn), the $\log \gamma D$–$\log fO_2$ slope is steeper than when uncorrected, and consistent with a 3+ valence for Sb in the silicate melt (Fig. 7). For this reason, all partition coefficients for Sb have been corrected using the calculated activity coefficients (Table 1); due to limited data, a necessary assumption is that the solution parameters are unchanged with pressure and temperature.

4.4.3. Temperature

The effect of temperature can be evaluated with the series of runs done at 1 GPa with basalt, from 1400 to 1800 °C (Fig. 9). These four runs illustrate an overall decrease in $D_{Sb}^{met/sil}$ with temperature and all other variables essentially constant (silicate melt composition, relative oxygen fugacity, and metal compositions). There are slight differences in metallic C content in these runs, but $X_C = 0.17$–0.19 for these four runs, which is not enough to cause a substantial variation in the partition coefficient given what is known in solid metal–liquid metal systems for Sb (e.g., Chabot et al., 2006). Temperature variations in the MgO capsules series are not evident, but the silicate melt and metallic liquid compositions are changing as is discussed below. Therefore the C capsule series is the most reliable

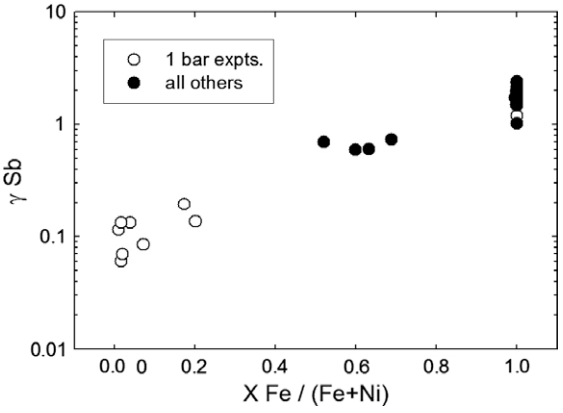

Fig. 8. Variation of activity coefficient (γ) for Sb with Fe/(Fe + Ni) molar ratio in FeNiSb metal in all runs from this study. One bar experiments are shown as open circles, and all other (higher pressure runs) are solid symbols. The variation from 0.06 to 2 has been applied to all partition coefficients in this study, and the magnitude of the correction is evident in Fig. 7 for the 1 bar experiments.

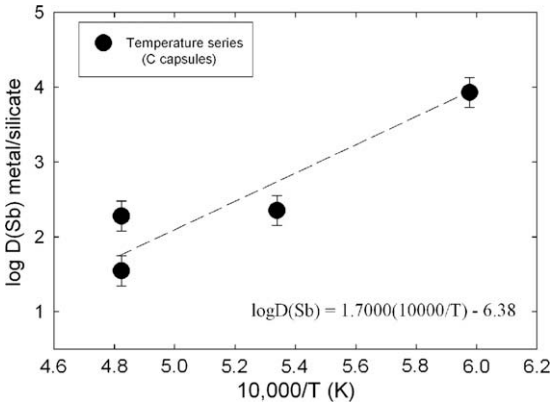

Fig. 9. Experiments carried out in graphite capsules at 1.5 GPa, and basaltic melt, but variable temperature (from 1400 to 1800 °C; experiments 7, 10, 11 and 15), illustrate the magnitude of the temperature effect on $D_{Sb}^{met/sil}$). The result of a linear fit to this series is displayed in the lower right corner of the graph.

to assess any temperature effect. This temperature effect can be fit with a linear expression (Fig. 9), and will be applied to natural examples below.

4.4.4. Silicate melt composition

Silicate melt composition and structure is known to influence the magnitude of metal/silicate partition coefficients (e.g., Walter et al., 2000). For antimony much previous work has been reported in the metallurgical literature. Nagamori et al. (1975) showed $D_{Sb}^{met/sil}$ decreases at higher temperatures, and also with higher Fe/SiO_2 (more basic or depolymerized melts), but since the studies were in Cu-rich systems and unusual silicate compositions, the results are difficult to apply to natural systems. Similarly, Font et al. (1999, 2000) showed that Sb has a preference for calcium ferrite slag over iron silicate slag, indicating strong melt compositional dependence to Sb solubility in silicate melts. Finally, Guo (2008) showed that Sb solubility in silicate melts was substantially decreased with addition of Al to silicate melts. Because silicate melt compositional variation can be extensive due to multiple components (Ca, Mg, Fe, Si, Al, Ti), a simple method to characterize structural and compositional changes is desirable. The parameter nbo/t, a gauge of silicate melt polymerization as a function of composition (Mysen, 1991; Mills, 1993), will be used here to make a preliminary evaluation of the magnitude of the effect of melt composition on $D_{Sb}^{met/sil}$. Its advantage is that it is straightforward to calculate for a wide range of silicate melts, but a disadvantage that will have to be accommodated is that it does not take into account potential coordination changes of various cations (e.g., Si and Al) at high pressure and temperature conditions.

Our series of experiments in Fe capsules at 1500 °C (Table 1) can be used to evaluate the effect of changing silicate melt composition. These experiments all have a slightly different oxygen fugacity, but can be compared assuming the valence is 3+ in this range, as determined in Section 4.4.3. To compare two experiments at the same temperature, but slightly different fO_2, a correction can be made

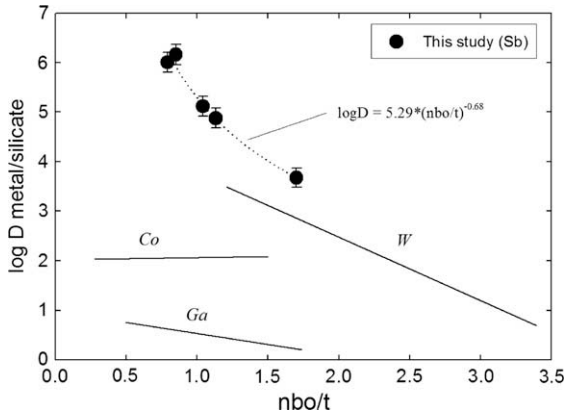

Fig. 10. $D_{Sb}^{met/sil}$ metal/silicate vs. nbo/t for a series of experiments at 1.0 GPa, 1500 °C, and variable melt composition (experiments 307, 309–312). The effect of slightly different oxygen fugacities between these five runs has been corrected using the slope of −0.75 correction (from Fig. 7). The magnitude of the silicate melt composition effect is compared to that of other elements such as Ga and Co (Jaeger and Drake, 2000) and W (Walter and Thibault, 1995). The results of an exponential fit to the data is displayed in the figure; slope for Sb is similar to that obtained for other high valence elements such as W, Mo and P (e.g., Walter et al., 2000).

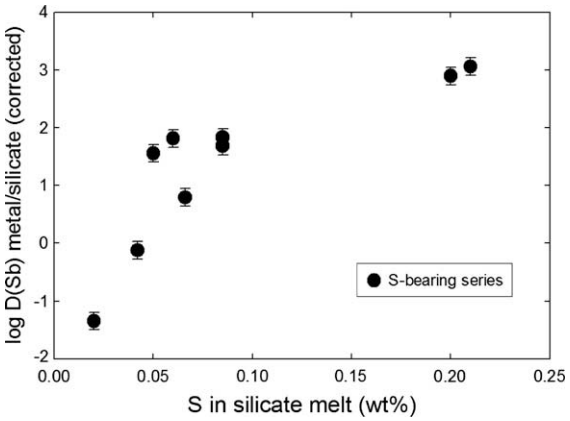

Fig. 11. Variation of $D_{Sb}^{met/sil}$ with S content (in ppm) in silicate melt (experiments 1–6, 8, 9, and 12). The higher S contents are associated with high D(Sb), suggesting Sb avoidance in the silicate melt with increasing S content.

by adding or subtracting by 0.75 × ln(fO_2 difference between experiments). After the correction for oxygen fugacity is made, a clear silicate melt compositional effect can be seen (Fig. 10). The experiment with the lowest $D_{Sb}^{met/sil}$ has the most basic silicate melt with the highest MgO and CaO, and lowest Al_2O_3 content. Linear fits to the data are possible, but result in an improbably large decrease in $D_{Sb}^{met/sil}$ at values of nbo/t close to that of molten peridotite. However, an exponential function results in a better fit ($r^2 = 0.983$), and causes a shallowing of the melt compositional effect at higher values of nbo/t. This result is entirely empirical, but given the dearth of data for $D_{Sb}^{met/sil}$ we will use this fit to extraplotate to natural perodititic melts in examples below, with the understanding that additional and more extensive studies should be carried out to explore these melt compositional effects.

The magnitude of the effect for Sb can be compared to other trace elements such as Co, Ga, and W, from previous studies (Walter and Thibault, 1995; Jaeger and Drake, 2000). The magnitude of the effect on antimony is as might be expected for a 3+ valence cation. For example, it is inferred from other work on siderophile trace elements that solubility in silicate melt is affected by changes due to complexing (e.g., Mo—Eggins and O'Neill, 2002) or coordination changes (Ni, Pd—Borisov et al., 2004). In the case of Sb, there is clear evidence from our dataset as well as previous studies (Guo, 2008) for Sb preferring more basic solutions that are CaO-, and MgO-rich and Al_2O_3-poor. The melts studied here are not particularly Na_2O or K_2O rich so complexing and speciation equilibria involving alkalis would seem less relevant than those involving network modifiers. It should be recognized that more detailed future work could explore differences between CaO and MgO-rich melts, since the effects of these network modifiers are not distinguished with a melt structural parameter such as nbo/t.

4.4.5. Pressure

Pressure is known to cause both increases and decreases in $D_i^{met/sil}$ but it is dependent upon temperature effects as well because most high P experiments are also at high T. The effect of pressure alone would be expected to cause an increase in $D_i^{met/sil}$ (such as Ni; Righter, 2003), but in many cases, the combination of P, T and fO_2 causes a decrease (e.g., Li and Agee, 1996). In the case of Sb, we can take advantage of the known effects of fO_2, temperature and melt composition to compare high pressure runs to look at (and isolate) a pressure effect. When experiments in graphite capsules and containing FeSb metallic liquids at 15, 120 and 130 kb are all corrected to 1800 °C, $\Delta IW = -2$, and nbo/t = 0.8 (using the fits from Figs. 7, 9 and 10), there is a small but clear pressure effect, resulting in a decrease over this large pressure range (Fig. 12). Again,

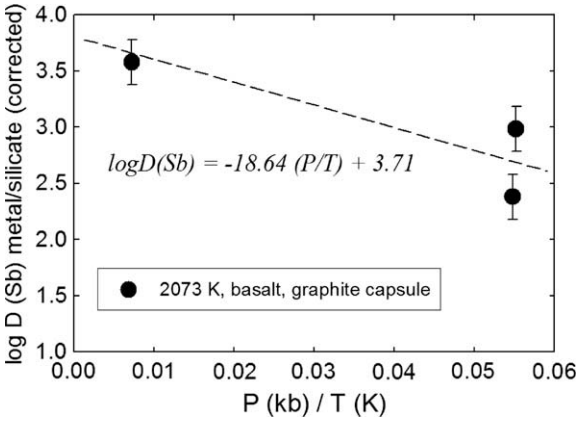

Fig. 12. Isolation of a pressure effect for $D_{Sb}^{met/sil}$ in experiments carried out in graphite capsules with basalt (experiments 11, 59, and 62), and corrected to 1800 °C (using expression from Fig. 9), and for small differences in fO_2. These three experiments were selected to minimize the amount and extent of correction needed for comparison. Resulting pressure effect for $D_{Sb}^{met/sil}$ is small and comparable to other siderophile elements such as Ni.

the decrease is similar to that measured for some other siderophile elements across this pressure range such as Ni (Li and Agee, 1996). As with other variables, this pressure effect can be fit with a simple linear expression, and will be applied to natural examples below.

4.4.6. Effects of C and S in silicate melt and metallic liquid

An important metal compositional effect is the influence of C or S content on element partitioning. The effect of sulfur on Sb partitioning in solid metal/liquid metal systems has been known for some time (e.g., Lodders and Palme, 1991), but recent studies have revealed systematic behavior (Chabot et al., 2003, 2006, in press). For example in the FeNiS system, Chabot et al. (2003) show that $D_{Sb}^{solid-metal/liquid-metal}$ increases by a factor of approximately 10 when the liquid metal is S-rich (30 wt.%) compared to S-free. Similarly, the Fe–C system exhibits large differences in SM/LM with a factor 6 increase in $D_{Sb}^{solid-metal/liquid-metal}$ in C-rich (~4 wt.%) compared to C-free systems (Chabot et al., 2006). These variations are also consistent with the sense of change obtained by Righter and Drake (2000) for $D_{Sb}^{met/sil}$ experiments that contained S-poor and S-rich metallic liquids.

In this study, we do not have experiments with a wide range of S content in the metallic liquid (MgO capsule series contains S = 0–5%; Table 2), so these effects cannot be evaluated systematically. However, for a series corrected for variable temperature, oxygen fugacity, and melt composition (using the corrections and fits discussed above for these variables), the remaining variable was silicate melt S content, and there is a dependence upon S content of the silicate melt. The highest *D*'s contained the highest S content in the silicate melt, and the lowest *D*'s contained the lowest (Fig. 11). This is a variable that must be explored in future studies, but also in systems containing higher S contents where the effect of S in metallic liquids can be even larger (e.g., Chabot et al., in press).

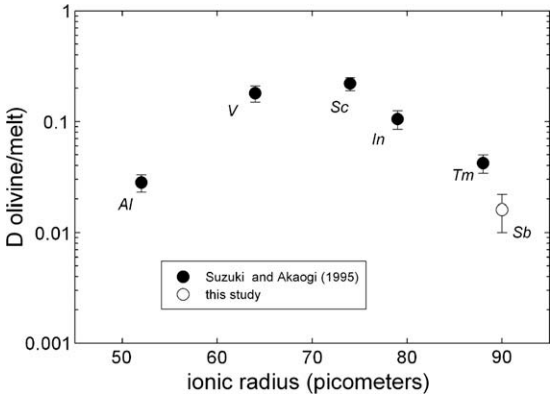

Fig. 13. Comparison of olivine/melt partition coefficients for trivalent ions Al, V, Sc, In and Tm (from Suzuki and Akaogi, 1995) to the measurement of D(Sb) olivine/melt from this study (experiment #5). The value for Sb plots along the trivalent parabola consistent with Sb^{3+} in these experiments. Ionic radii are from Shannon (1976).

5. DISCUSSION

5.1. Mineral/melt partitioning of Sb

Incompatible behavior is expected for Sb, due to its correlation with other incompatible elements such as Pr (Jochum and Hofmann, 1997), but it is important to define because some volatile elements may be more compatible than others (e.g., Witt-Eickschen et al., 2007), making the volatility trend (Fig. 1) difficult to interpret. For olivine, there are some previous studies that help interpret our new data for Sb (e.g., Suzuki and Akaogi, 1995). The $D_{Sb}^{met/sil}$ values of 0.016 measured in this study are consistent with the values expected from correlations with ionic radii of some 3+ ions (Fig. 13). Together with the trend from these other 3+ elements there is additional evidence for 3+ stability for Sb. Pyroxene/melt partition coefficients are not as systematically understood, but the value measured here—0.18—is mildly incompatible and similar to that measured for Re (Righter and Hauri, 1998). These results suggest that Sb is mildly to highly incompatible during melting of a silicate mantle.

5.2. Tin and phosphorus

The origin of Sn and P depletions in Earth may be evaluated with the new experimental data. Previous high pressure and temperature $D_{Sn}^{met/sil}$ data (from Righter and Drake, 2000) did not include effects of S or C in the metal phase, but now there are new experiments that contain both of these light elements. In addition, the studies of Capobianco et al. (1999) cover effects of fO_2 and melt composition at 1 bar. The high pressure and temperature studies of Righter and Drake (2000) and this study help to constrain the effects of variable *P* and *T* with a range of experiments between 1300 and 2150 °C, and 1.0 and 15.0 GPa. And finally the latter studies also explore the effect of metallic liquids with S and C dissolved.

Phosphorus partition coefficients in this study can be combined with previous results (Newsom and Drake, 1983; Schmitt et al., 1989; Young et al., 1992; Hillgren, 1993; Walker et al., 1993; Hillgren et al., 1996; Righter et al., 1997; Jana and Walker, 1997a,b; Righter and Drake, 1999, 2000). We have chosen to quantify the effects of silicate melt composition on $D_P^{met/sil}$ using both nbo/t and oxide mole fractions—X_{SiO_2}, X_{MgO}, X_{CaO}, $X_{Al_2O_3}$, and X_{FeO}. This is for two reasons: (1) the oxide mole fraction approach works well if there are many data across a wide compositional range with which to calibrate and in the case of P there ~100 experiments, and (2) nbo/t does not discriminate between CaO and MgO, both network modifiers in the silicate melt, and important to distinguish since the mantle is made mostly of MgO. In addition, the studies of Newsom and Drake(1983), Schmitt et al.(1989), Hillgren (1993) cover the effects of fO_2 and temperature at 1 bar. The high pressure studies of Walker et al (1993), Hillgren et al. (1996), Righter and Drake (2000) and this study help to constrain the effects of pressure variation. The Young et al. (1992) and Jana and Walker (1997a) were done with variable melt compositions. And finally the experiments

of Hillgren (1993), Jana and Walker (1997b), Righter and Drake (2000), and this study constrain the roles of S and C.

Calculation of metal–silicate partition coefficients as a function of all these variables have been possible using an approach guided by chemical thermodynamics where:

$$(1)\ \ln D_P^{met/sil} = a\ln fO_2 + b/T + cP/T + d(1-Xs) + e(1-Xc) + \sum f_i X_i + g \quad \text{and}$$

$$\ln \gamma D_{Sn}^{met/sil} = a\ln fO_2 + b/T + cP/T + d(1-Xs) + e(1-Xc) + f(nbo/t) + g.$$

The a, b, c, and g terms relate to valence, enthalpy (H/RT), volume (VP/RT), and entropy (S/R), and the d and e terms to activity expressions for these elements in a metallic liquid. The f terms relate to the silicate melt composition. The f terms have sometimes been regressed against nbo/t, but it has become clear that this term is not a completely satisfactory parameter in gauging melt compositional effects where CaO and MgO, for example, both network modifiers, have differing effects of D (e.g., Eggins and O'Neill, 2002). Here we use nbo/t to assess the effect of melt composition on $D_P^{met/sil}$ and $D_{Sn}^{met/sil}$, and also use oxide mole fractions for $D_P^{met/sil}$ since melt compositional effects for the latter are so severe for highly charged cations like P (e.g., Righter, 2003).

Comparison of calculated to measured $D_{Sn}^{met/sil}$ and $D_P^{met/sil}$ for approximately 60 and 100 experiments, respectively, shows good agreement (Fig. 14), with a few exceptions. The results of the multiple linear regression are much better for $D_P^{met/sil}$ when oxide mole fractions are used and shows the ability of this approach to distinguish between individual cations that might have different thermodynamic or structural properties than others. When $D_P^{met/sil}$ is calculated using either approach (nbo/t vs. oxide mole fractions) the resulting Ds are the same, except the er-

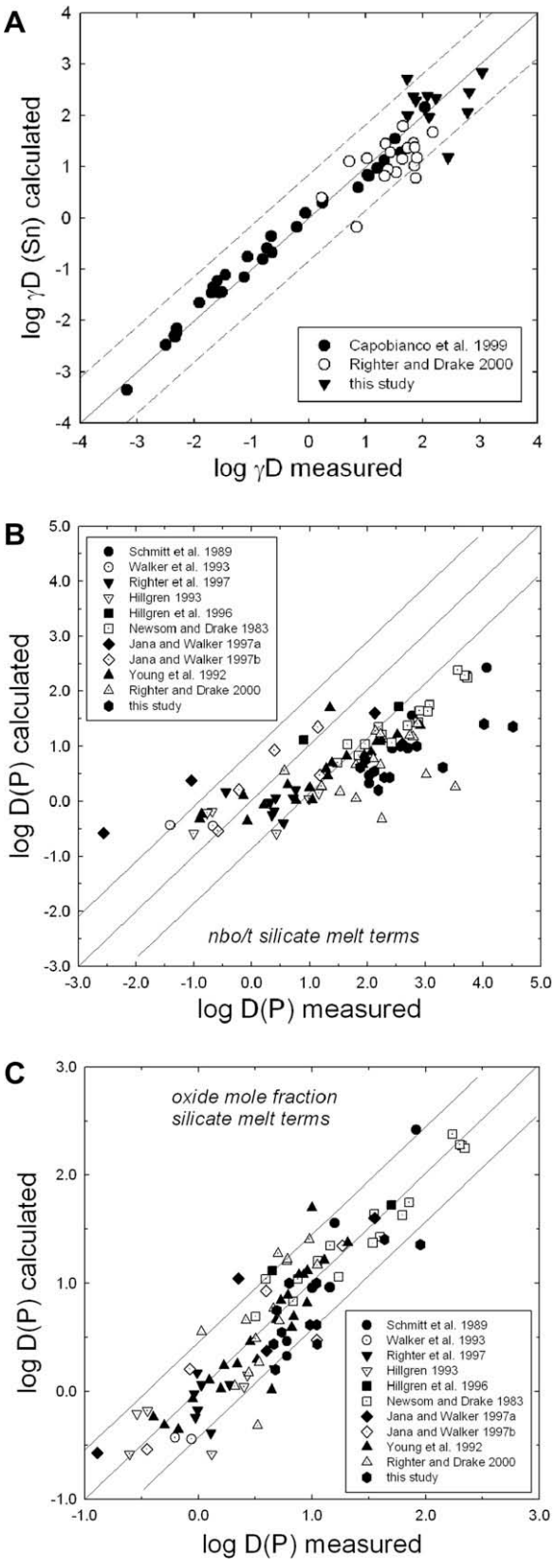

Fig. 14. (A) Results of multiple linear regression of $\gamma D_{Sn}^{met/sil}$ experiments in this study and the literature. Regression results have an r^2 value of 0.947, and $a = -0.979$ (0.044), $b = 59300$ (3070), $c = 150$ (18), $d = -7.55$ (1.20), $e = -4.88$ (2.18), $f = -0.267$ (0.281), and $g = 13.77$ (1.82) (values in parentheses are 1 sigma error). Error on the calculated $\ln\gamma D_{Sn}^{met/sil}$ is 0.95. Previous studies included in the regression are: Capobianco et al. (1999) and Righter and Drake (2000). Gamma (γ) corrections for metal composition are explained in detail in Capobianco et al. (1999) and Righter and Drake (2000). (B) Results of multiple linear regression analysis for $D_P^{met/sil}$ experiments, using nbo/t term for silicate melt composition. Regression results have an r^2 value of 0.64, and $a = -0.531$ (0.066), $b = -34670$ (4000), $c = 71.8$ (17.4), $d = 5.94$ (1.56), $e = 6.05$ (1.69), $f = -1.21$ (0.15), and $g = 10.87$ (1.38). Error on the calculated $\ln D_P^{met/sil}$ is 1.07. (C) Results of multiple linear regression analysis for $D_P^{met/sil}$ experiments, using oxide mole fraction terms for silicate melt composition. Regression results have an r^2 value of 0.85, and $a = -0.677(0.067)$, $b = 51200$ (5250), $c = 82$ (14), $d = 6.92$ (1.18), $e = 5.45$ (1.31), $f_{SiO_2} = 44.7(4.9)$, $f_{MgO} = 31.2(4.2)$, $f_{CaO} = 33.0(4.3)$, $f_{Al_2O_3} = 49.5(4.9)$, $f_{FeO} = 32.0(4.2)$, and $g = -23.3(4.2)$. Error on the calculated ln $D_P^{met/sil}$ is 0.80. Previous studies included in both of the $D_P^{met/sil}$ regressions are: 1600 °C experiments of Newsom and Drake (1983), Schmitt et al. (1989), Young et al. (1992), Hillgren (1993), Walker et al. (1993), Hillgren et al. (1996), Righter et al. (1997), Jana and Walker (1997a,b), Righter and Drake (1999, 2000).

ror is much smaller using oxide mole fractions (see application below to Earth). The negative terms for S and C in the regression for D(Sn) indicate that addition of these light elements to the metallic liquid cause an increase in the partition coefficient. The direction and magnitude of change is in agreement with the suggestions of Righter and Drake (2000) in which they saw large increases in $D_{Sn}^{met/sil}$ with addition of S, but relatively small to no change with addition of C. The increase in the D(M/S) is opposite to that observed in solid metal/liquid metal systems for Sn, where D(SM/LM) increases with S and C, indicating a preference for the solid. However, the addition of silicate melt in this case undoubtedly changes this behavior such that the Sn avoids S-bearing silicate melt. Similar behavior is observed in this study for Sb (see 4.3g above), and this phenomenon deserves further study.

Application of the results can be made to the Earth and Moon. Calculations for a deep magma ocean for the early Earth (25 GPa, 2100 °C, $\Delta IW = -1.5$, $Xs = X_C = 0.1$; peridotitic silicate melt; e.g., Righter, 2003) yield $D_{Sn}^{met/sil} = 70$ (+100/−45) and $D_P^{met/sil} = 1.9$ (+3.6/−1.3) (nbo/t) or 2.2 (+2.6/−1.2) (oxide mole fraction), in agreement with previous assessments that the volatility corrected depletions of Sn and P are due to moderately siderophile behavior at these conditions. The agreement between $D_P^{met/sil}$ calculated using nbo/t or oxide mole fractions indicates that the results of Sn and Sb modelling below are internally consistent with the modelling results here for P. Similarly, application of the results to the Moon show that $D_P^{met/sil}$ calculated for conditions of 4.5 GPa, 1900 °C, $\Delta IW = -2.2$, $Xs = X_C = 0$ (e.g., Righter, 2002), result in a value of 4.5–5.5. These $D_P^{met/sil}$ are slightly higher than that calculated for the early Earth, but the small metallic lunar core (<2 mass%) would not be a strong lever on the lunar mantle, resulting only in a very small lowering of P in the lunar mantle (see also Righter, 2002). Sparse data for Sn in lunar samples precludes application of our results to the lunar core. In summary, these results are consistent with the idea that the Earth and Moon both experienced hot early differentiation events.

5.3. Behavior of Sb during mantle melting—volatility and sulfide retention

Concentrations of Sb in basaltic rocks are controlled by several processes: melting with or without sulfide saturation, and also volatility. During melting of a mantle without sulfide present, Sb will behave incompatibly and melts and residua will define a linear array as they do for elements such as W and Mo in planetary basalt (e.g., Wänke, 1981). However, Sb has a high partition coefficient between sulfide liquid and silicate melt, so that retention of small amount of sulfide in the residual mantle would cause lower Sb concentrations in basaltic melts, such as those in some MORB (Fig. 2). An additional contribution to lower concentrations is that Sb is a volatile element and is probably lost during magmatic degassing, such as in many lunar basalts (Fig. 2). Both of these characteristics—magmatic volatility and chalcophility—are shared by the element Re which serves as an example of similar behavior to Sb (e.g., Bennett et al., 2000; Righter et al., 2008b). Nonetheless, those lunar basalts exhibiting the highest Sb concentrations (and thus melted from a mantle without sulfide and experienced little volatility loss) are still depleted by a factor of ~50 relative to terrestrial basalt (Fig. 2). Using the slope exhibited by the well-defined array of terrestrial basalts, komatiites, and peridotite, the lunar mantle Sb content can be estimated from the basalts, as illustrated in Fig. 2.

5.4. Implications for Sb in the mantle of the Earth

The origin of Sb depletions in Earth and Moon mantles may be evaluated with the new experimental data. Abundances of Sb in the Earth's mantle (e.g., Jochum and Hofmann, 1997) indicate a depletion of approximately 7 ± 1 (relative to chondrites, and accounting for volatility since the position of Sb along the volatility trend in Fig. 1 reduces the depletion by a factor of $\sim 7 \pm 1$). If this depletion has been caused by metal–silicate equilibrium in the Earth, a metal–silicate partition coefficient of 6 ± 1 is required. The results of our experiments can be used to evaluate the possibility that the terrestrial mantle depletion is due to metal–silicate equilibrium at the base of a deep magma ocean. For example, the effect of silicate melt composition can be evaluated for basaltic to peridotitic silicate melts, of high relevance to the issue of an early terrestrial or lunar magma ocean. Similarly the effects of high temperature and pressure can be evaluated using our new results. A popular scenario for core formation in the early Earth is that metal droplets and silicate melt equilibrated rapidly in a deep, convecting magma ocean. Proposed depths vary from the low end of 15–25 GPa and 1900–2100 °C up to the high end of 40–60 GPa and 2500–3000 °C (e.g., Righter, 2003; Wood et al., 2006).

Although we do not present enough data to carry out a multiple linear regression analysis of the $D_{Sb}^{met/sil}$ data, we can use a simplified extrapolation to estimate the magnitude of $D_{Sb}^{met/sil}$ at magma ocean conditions. For example, starting with a $D_{Sb}^{met/sil}$ determined in a relatively low pressure experiment, #309, we have $\gamma D_{Sb}^{met/sil} = 1.45 \times 10^6$ (conditions are 1500 °C, 1.0 GPa, nbo/t = 0.95, and $\Delta IW = -2.14$). This experiment represents the highest $D_{Sb}^{met/sil}$ measured in this study. Knowing the effect of fO_2, temperature, pressure, and melt composition from Figs. 7, 9, 10 and 12, this low PT experiment can act as an "anchor point" for extrapolation to conditions proposed for a magma ocean. Using this approach, $D_{Sb}^{met/sil}$ of ~5 can be calculated at $\Delta IW = -1.5$, 2100 °C, 25 GPa, and nbo/t = 2.5 (peridotite liquid with 500 ppm S). If the Earth is made of CI1 chondrites, with a bulk Sb content of 140 ppb, segregation of a 32 mass% core (x) and $D_{Sb}^{met/sil} = 5$, consideration of the simple equation:

$$C_{Sb}^{sil} = \frac{C_{Sb}^{bulk}}{\left[x + (1-x)\left(D_{Sb}^{met/sil}\right)\right]} \quad (1)$$

results in a mantle concentration of 9 ppb Sb (Fig. 15). The uncertainty associated with our extrapolation approach is higher than estimates of D for other more well studied ele-

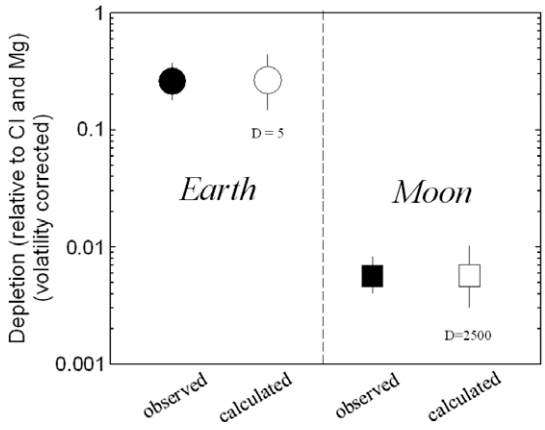

Fig. 15. Comparison of measured and calculated Sb depletions for the primitive upper mantle of the Earth and the Moon. The small terrestrial Sb depletion can be matched with calculations using $D_{Sb}^{met/sil} = 5$ (±3), and a core that is 32% of the mass of the Earth. The effect of $D_{Sb}^{met/sil}$ on the magnitude of the calculated lunar depletion is illustrated for $D = 2500$ (±1000). The value of 2500 results in a depletion identical to that deduced from Apollo samples, and for a lunar core of 2% of the mass. Earth depletions are calculated from data of Jochum and Hofmann (1997), and lunar depletions are calculated from data of Wolf et al. (1979) and Wolf and Anders (1980) (Table 4). Depletions have been normalized to Mg and CI chondrite values (from Newsom, 1995).

ments $D_{Sb}^{met/sil} = 5 \pm 3$), the resulting mantle concentrations are 9 ± 6 ppb, compared to estimates of 8–11 ppb Sb in the Earth's primitive upper mantle (Jochum and Hofmann, 1997). Thus it seems that Sb could easily be explained by an intermediate depth magma ocean scenario.

Li and Agee (2001), Chabot et al. (2005) and Wade and Wood (2005) propose that the siderophile elements Ni, Co, Cr, V and Mn can be explained at high PT magma ocean conditions of 40–60 GPa and 3000–3500 °C. Our results would predict no depletion of Sb in the terrestrial mantle (since $D_{Sb}^{met/sil} << 1$ at higher PT conditions), but this would require extrapolation well outside the current experimental database. Wade and Wood (2005) and Wood et al. (2008) propose that fO_2 increases during planetary growth. Increasing fO_2 would also produce $D_{Sb}^{met/sil}$ that is to low to be consistent with mantle abundances. It seems unavoidable that $D_{Sb}^{met/sil}$ would become too low at higher PT conditions to be consistent with an equilibrium scenario. On the other hand, as shown above, an intermediate depth magma ocean can explain Sb adequately.

5.5. Implications for Sb in the mantle of the Moon

One of the more interesting features of the lunar mantle is that many of the volatile elements are depleted to even lower levels than the Earth's mantle (Wolf et al., 1979; Wolf and Anders, 1980). In fact, Sb is a factor of 50 ± 5 lower in the Moon's mantle, than Earth's mantle. Formation models for the Moon include scenarios in which the Moon is derived from the mantle of a Mars-sized impactor (e.g., Cameron, 2000; Canup, 2004, 2008), which had most likely differentiated into a core and mantle. Although there is thus uncertainty as to the lunar bulk composition, such a large and differentiated impactor may have been made of material similar to Earth's primitive upper mantle (arguably so given that the impactor was large and probably hot enough to melt, as apparently did the early Earth), and a reasonable estimate (or at least a starting point for modelling) for the Sb concentration in the bulk Moon might be approximately 10 ppb. This approach has been used for other elements such as Ni, Co, and W, and in which the Moon forms from the mantle of a hot impactor, and then later (after re-accretion into the Moon) forms a small (2 mass%) metallic core (e.g., Righter, 2002).

Using the same extrapolation approach as used for the Earth in Section 5.4 (using experiment # 309 as an anchor), results in calculation of $D_{Sb}^{met/sil}$ of 2500 for conditions of $\Delta IW = -2.2$, 1900 °C, 4.5 GPa, 2.5 nbo/t (peridotite with 650 ppm S). These conditions are those proposed by Righter (2002) for equilibration between a small metallic core at high temperatures, and pressures near the center of the Moon (4.5 GPa), which can explain many other moderately siderophile elements in the lunar mantle such as Ni, Co and Mo. Using this partition coefficient value and consideration of Eq. (1), with a small metallic core (2%), and a bulk Sb content for the Moon of 10 ppb, results in Sb content for the lunar mantle of 0.0.20 ppb, or a factor of ~50 lower than the Earth's mantle concentration (Fig. 15). The uncertainty in the lunar Sb depletion of 50 ± 5 relative to Earth's mantle corresponds to an $D_{Sb}^{met/sil} = 2500 \pm 300$ (or a lunar mantle Sb content of 0.20 ± 0.03 ppb). The uncertainty in $D_{Sb}^{met/sil}$ using our extrapolation approach is greater than $D_{Sb}^{met/sil} = 2500 \pm 1000$) the natural constraints, corresponding to a lunar mantle Sb content of 0.20 ± 0.08 ppb. This result is not a unique set of conditions that can explain the data, but rather demonstrates consistency with previous work on moderately siderophile elements for a hot impactor scenario (Righter, 2002). The resulting $D_{Sb}^{met/sil}$, which is higher than the value calculated for the application to Earth's mantle, is attributed mainly to lower P and T conditions, relative to those for equilibrium in the terrestrial mantle, but is also related to the slightly lower oxygen fugacity for the Moon (relative to the Earth).

6. CONCLUSIONS

We have carried out a series of experiments to isolate several variables such as oxygen fugacity, temperature,

Table 4
Summary of Sb and Pr data used to estimate Sb concentrations in the Earth and Moon mantles.

	Sb (ppb)	Pr (ppm)	Data sources
CI chondrites	142 ± 10	0.089	Newsom (1995)
Earth's mantle (PUM)	9 ± 1	0.2	Jochum and Hofmann (1997), Schmidt et al. (2003)
Moon's mantle	0.20 ± 0.04	0.25	Wolf et al. (1979), Wolf and Anders (1980)

pressure, and silicate and metallic melt compositions. The activity of Sb in FeNi metal is strongly composition dependent such that solubility of Sb as a function of fO_2 must be corrected for the metal composition. When the correction is applied, Sb solubility is consistent with 3+ valence. Temperature series shows that $D_{Sb}^{met/sil}$ decreases by a factor of 100 over 400 °C, whereas a pressure series exhibits a substantial decrease between ambient pressure 100 MPa and 13 GPa. A strong dependence upon silicate melt composition is evident from a factor of ~100 decrease in $D_{Sb}^{met/sil}$ between nbo/t values of 0.3 and 1.7. Consideration of all these variables indicates that the small Sb depletion for the Earth's mantle can be explained by high PT equilibrium partitioning between metal and silicate melt, where $D_{Sb}^{met/sil} = 5$. The relatively large lunar Sb depletion can also be explained by segregation of a small (2%) metallic core, but with a much higher $D_{Sb}^{met/sil} = 2500$.

An explanation for the small Sb depletion in the terrestrial mantle only requires high PT equilibrium metal–silicate partitioning, rather than addition of late chondritic "veneer", as suggested by some studies for some of the volatile siderophile elements (e.g., Yi et al., 2000). Explanation for the lunar mantle depletion of Sb requires only segregation of a small lunar core following Moon formation, and not any additional loss due to volatility during or after the impact, as might be expected in a hot Earth–Moon post impact disk (Pahlevan and Stevenson, 2007). Thus, the volatile, siderophile elements can provide additional constraints on formation scenarios for the Earth and Moon.

ACKNOWLEDGMENTS

This research was carried out over a number of years, supported by NASA grants to MJD, MH, and KR, with experiments done at University of Arizona and NASA Johnson Space Center. We thank J. Collins and C. Capobianco for carrying out the experiments in the JC series samples, which were done as part of a student project, and to C. Capobianco for getting the first author interested in Sb. Thanks are due to E.K. Gibson, Jr., for providing C steel standards, K. Domanik, L. Le, and A. Peslier for assistance with the electron microprobe, and to S. Huang with assistance with the LA-ICP-MS at FSU. Journal reviews of H. Palme, E. Cottrell, and an anonymous reviewer, as well as the comments of AE B. Mysen, helped to clarify the presentation considerably.

REFERENCES

Bennett V. C., Norman M. D. and Garcia M. O. (2000) Rhenium and platinum group element abundances correlated with mantle source components in Hawaiian picrites: sulfides in the plume. *Earth Planet. Sci. Lett.* **183**, 513–526.

Borisov A., Lahaye Y. and Palme H. (2004) The effect of TiO_2 on Pd, Ni, and Fe solubilities in silicate melts. *Am. Mineral.* **89**, 564–571.

Boynton W. V. and Hill D. (1983) Composition of bulk samples and a possible pristine clast from Allan Hills A81005. *Geophys. Res. Lett.* **10**, 837–840.

Cameron A. G. W. (2000) High resolution simulations of the giant impact. In *Origin of the Earth and Moon* (eds. R. M. Canup and K. Righter). Univ. of Arizona Press, Tucson, Arizona, pp. 133–144.

Campbell A. J. and Humayun M. (1999) Trace element microanalysis in iron meteorites by laser ablation ICPMS. *Anal. Chem.* **71**, 939–946.

Campbell A. J., Humayun M. and Weisberg M. K. (2002) Siderophile element constraints on the formation of metal in the metal-rich chondrites Bencubbin, Weatherford, and Gujba. *Geochim. Cosmochim. Acta* **66**, 647–660.

Canup R. M. (2004) Simulations of a late lunar-forming impact. *Icarus* **168**, 433–456.

Canup R. M. (2008) Implications of lunar origin via giant impact for the Moon's composition and the thermal state of the proto-Earth. *Lunar Planet. Sci.* **XXXIX**, 2429.

Capobianco C. J., Drake M. J. and DeAro J. (1999) Siderophile geochemistry of Ga, Ge, and Sn: cationic oxidation states in silicate melts and the effect of composition in iron-nickel alloys. *Geochim. Cosmochim. Acta* **64**, 3581–3597.

Chabot N. L., Campbell A. J., Jones J. H., Humayun M. and Agee C. B. (2003) An experimental test of Henry's Law in solid metal–liquid metal systems with implications for iron meteorites. *Met. Planet. Sci.* **38**, 181–196.

Chabot Nancy L., Draper David S. and Agee Carl B. (2005) Conditions of core formation in the Earth: constraints from nickel and cobalt partitioning. *Geochim. Cosmochim. Acta* **69**, 2141–2151.

Chabot N. L., Campbell A. J., Jones J. H., Humayun M. and Lauer, Jr., H. V. (2006) The influence of carbon on trace element partitioning behavior. *Geochim. Cosmochim. Acta* **70**, 1322–1335.

Chabot N.L., Saslow S.A., McDonough W.F. and Jones J.H. (in press) An investigation of the behavior of Cu and Cr during iron meteorite crystallization. *Met. Planet. Sci.* **44**.

Cheng W. and Ganguly J. (1994) Some aspects of multicomponent excess free energy models with subregular binaries. *Geochim. Cosmochim. Acta* **58**, 3763–3767.

Claussen O., Gerlach S. and Russel C. (1999) Self-diffusivity of polyvalent ions in silicate liquids. *J. Non-Crystal. Solids* **253**, 76–83.

Eggins S. M. and O'Neill H. St. C. (2002) The effect of melt composition on trace element partitioning: an experimental investigation of the activity coefficients of FeO, NiO, CoO, MoO_2 and MoO_3 in silicate melts. *Chem. Geol.* **186**, 151–181.

Ertel W., O'Neill H. St. C., Sylvester P. J., Dingwell D. B., Sylvester P. J. and Spettel B. (2001) The solubility of rhenium in silicate melts: implications for the geochemical properties of rhenium at high temperatures. *Geochim. Cosmochim. Acta* **65**, 2161–2170.

Ertel W., Dingwell D. B. and Sylvester P. J. (2008) Siderophile elements in silicate melts—A review of the mechanically assisted equilibration technique and the nanonugget issue. *Chem. Geol.* **248**, 119–130.

Filiberto J., Treiman A. H. and Le L. (2007) Crystallization experiments on a Gusev basalt composition. *Meteorit. Planet. Sci.* **43**, 1137–1146.

Font J. M., Hino M. and Itagaki K. (2000) Phase equilibrium and minor element distribution between Ni_3S_2–FeS matte and calcium ferrite slag under high partial pressures of SO_2. *Metall. Mater. Trans.* **31B**, 1231–1239.

Font J. M., Hino M. and Itagaki K. (1999) Phase equilibrium and minor elements distribution between iron–silicate base slag and nickel–copper–iron matte at 1573 K under high partial pressures of SO_2. *Mater. Trans. Jpn. Inst. Metals* **40**, 20–26.

Guo Q. (2008) Some aspects of arsenic and antimony geochemistry in high temperature granitic melt—aqueous fluid system and in low temperature permeable reactive barrier—groundwater system. Ph.D. Thesis, Univ. Waterloo, Ont., Canada, 175 pp.

Gupta K. P. (2000) The Co–Ni–Sb system. *J. Phase Equilib.* **21**, 472–478.

Gustafson P. (1985) A thermodynamic evaluation of the C–Fe system. *Scand. J. Metall.* **14**, 259–267.

Hill D. H., Boynton W. V. and Haag R. A. (1991) A lunar meteorite found outside the Antarctic. *Nature* **352**, 614–617.

Hillgren V.J. (1993) Partitioning behavior of moderately siderophile elements in Ni-rich systems: implications for the Earth and Moon. Ph.D. Thesis. Univ. Ariz. 423 pp.

Hillgren V. J., Drake M. J. and Rubie D. C. (1996) High pressure and high temperature metalsilicate partitioning of siderophile elements: the importance of silicate liquid composition. *Geochim. Cosmochim. Acta* **60**, 2257–2263.

Holzheid A., Palme H. and Chakraborty S. (1997) The activities of NiO, CoO and FeO in silicate melts. *Chem. Geol.* **139**, 21–38.

Humayun M. and Clayton R. N. (1995) Potassium isotope cosmochemistry: genetic implications of volatile element depletion. *Geochim. Cosmochim. Acta* **59**, 2131–2148.

Humayun M., Simon S. B. and Grossman L. (2007) Tungsten and hafnium distribution in calcium–aluminum inclusions (CAIs) from Allende and Efremovka. *Geochim. Cosmochim. Acta* **71**, 4609–4627.

Jaeger W. L. and Drake M. J. (2000) Metal–silicate partitioning of Co, Ga, and W: dependence on silicate melt composition. *Geochim. Cosmochim. Acta* **64**, 3887–3895.

Jana D. and Walker D. (1997a) The influence of silicate melt composition on distribution of siderophile elements among metal and silicate liquids. *Earth Planet. Sci. Lett.* **150**, 463–472.

Jana D. and Walker D. (1997b) The influence of sulfur on partitioning of siderophile elements. *Geochim. Cosmochim. Acta* **61**, 5255–5277.

Jochum K. P. and Hofmann A. W. (1997) Constraints on earth evolution from antimony in mantle-derived rocks. *Chem. Geol.* **139**, 39–49.

Jones J. H. and Drake M. J. (1986) Geochemical constraints on core formation in the Earth. *Nature* **322**, 221–228.

Kress V. C. and Carmichael I. S. E. (1991) The compressibility of silicate liquids containing Fe_2O_3 and the effect of composition, temperature, oxygen fugacity and pressure on their redox states. *Contrib. Mineral. Petrol.* **108**, 82–92.

LaTourrette T., Wasserburg G. J. and Fahey A. J. (1996) Self diffusion of Mg, Ca, Ba, Nd, Yb, Ti, Zr, and U in haplobasaltic melt. *Geochim. Cosmochim. Acta* **60**, 1329–1340.

Leinenweber K., Mosenfelder J., Diedrich T., Soignard E., Sharp T., Tyburczy J. and Wang Y. (2006) High-pressure cells for in situ multi-anvil experiments. *High Press. Res.* **26**, 283–292.

Li J. and Agee C. B. (1996) Geochemistry of mantle-core formation at high pressure. *Nature* **381**, 686–689.

Li J. and Agee C. B. (2001) The effect of pressure, temperature, oxygen fugacity and composition on partitioning of nickel and cobalt between liquid Fe–Ni–Sb alloy and liquid silicate: Implications for the Earth's core formation. *Geochim. Cosmochim. Acta* **65**, 1821–1832.

Lodders K. and Palme H. (1991) The role of sulfur in planetary core formation. *Meteoritics* **26**, 366.

McDonough W. F. and Sun S.-S. (1995) Composition of the Earth. *Chem. Geol.* **120**, 223–253.

Mills K. C. (1993) The influence of structure on the physicochemical properties of slags. *ISIJ Int.* **33**, 148–155.

Morgan J. W., Higuchi H., Takahashi H. and Hertogens J. (1978) A "chondritic" eucrite parent body: inferences from trace elements. *Geochim. Cosmochim. Acta* **42**, 27–38.

Mukhopadhyay B., Basu S. and Holdaway M. J. (1993) A discussion of Margules-type formulations for multicomponent solutions with a generalized approach. *Geochim. Cosmochim. Acta* **57**, 277–283.

Mysen B. O. (1991) Volatiles in magmatic liquids. In *Physical Chemistry of Magma* (eds. L. L. Perchuk and I. Kushiro). Cambridge University Press, New York, pp. 435–476 (Chapter 16).

Nagamori M., Mackey P. and Tarassoff P. (1975) Copper solubility in FeO–Fe_2O_3–SiO_2–Al_2O_3 slag and distribution equilibria of Pb, Bi, Sb, and As between slag and metallic copper. *Metall. Trans.* **6B**, 295–301.

Newsom H. E. (1984) The lunar core and the origin of the Moon. *EOS* **65**, 369–370.

Newsom H. E. (1995). In *Global Earth Physics: A Handbook of physical constants: AGU Reference Shelf volume 1* (ed. T. J. Ahrens). AGU, Washington, pp. 159–189.

Newsom H. E. and Drake M. J. (1983) Experimental investigations of the partitioning of phosphorus between metal and silicate phases: implications for the Earth, Moon and eucrite parent body. *Geochim. Cosmochim. Acta* **47**, 93–100.

Newsom H. E. and Sims K. W. W. (1991) Core formation during early accretion of the Earth. *Science* **252**, 926–933.

Newsom H. E., White W. M., Jochum J. P. and Hofmann A. W. (1986) Siderophile and chalcophile element abundances in oceanic basalts, Pb isotope evolution and growth of the Earth's core. *Earth Planet. Sci. Lett.* **80**, 299–313.

Noll P. D., Newsom H. E., Leeman W. P. and Ryan J. G. (1996) The role of hydrothermal fluids in the production of subduction zone magmas: evidence from siderophile and chalcophile elements and boron. *Geochim. Cosmochim. Acta* **60**, 587–611.

Ohtani E., Yurimoto H. and Seto S. (1997) Element partitioning between metallic liquid, silicate liquid, and lower-mantle minerals: implications for core formation of the Earth. *Phys. Earth Planet. Int.* **100**, 97–114.

Okamoto H. (1999) Fe–Sb system. *J. Phase Equilib.* **20**, 166.

O'Neill H. St. C., Berry A. J. and Eggins S. M. (2008) The solubility and oxidation state of tungsten in silicate melts: implications for the comparative chemistry of W and Mo in planetary differentiation processes. *Chem. Geol.* **255**, 346–359.

Pahlevan K. and Stevenson D. (2007) Equilibration in the aftermath of the lunar-forming giant impact. *Earth Planet. Sci. Lett.* **262**, 438–449.

Pei B., Bjorkman B., Sundman B. and Janson B. (1995) Thermodynamic assessment of the iron-antimony system. *Calphad* **19**, 1–15.

Pouchou J.-L. and Pichoir F. (1991) Quantitative analysis of homogeneous or stratified microvolumes applying the model "PAP". In *Electron Microprobe Quantitation* (eds. K. F. J. Heinrich and D. E. Newbury). Plenum Press, New York, pp. 31–75.

Raghavan V. (2004) Fe–Ni–Sb system. *J. Phase Equilib. Diffusion* **25**, 89–91.

Righter K. (2002) Does the Moon have a metallic core? Constraints from giant impact modelling and siderophile elements. *Icarus* **158**, 1–13.

Righter K. (2003) Metal–silicate partitioning of siderophile elements and core formation in the early Earth and terrestrial planets. *Ann. Rev. Earth Planet. Sci.* **31**, 135–174.

Righter K. (2005) Highly siderophile elements: constraints on Earth accretion and early differentiation. In *Structure, Composition and Evolution of Earth's mantle 160* (eds. J. Bass, R. van der Hilst, J. Matas and J. Trampert). AGU Monograph Series, pp. 201–218.

Righter K. (2007) Not so rare Earth? New developments in understanding the origin of the Earth and Moon. *Chem. Erde* **67**, 179–200.

Righter K. and Drake M. J. (1999) Effect of water on metal–silicate partitioning of siderophile elements: a high pressure and temperature terrestrial magma ocean and core formation. *Earth Planet. Sci. Lett.* **171**, 383–399.

Righter K. and Drake M. J. (2000) Metal/silicate equilibrium in the early Earth: new constraints from the volatile moderately siderophile elements Ga, Cu, P and Sn. *Geochim. Cosmochim. Acta* **64**, 3581–3597.

Righter K. and Hauri E. H. (1998) Compatibility of rhenium in garnet during mantle melting and magma genesis. *Science* **280**, 1737–1741.

Righter K., Drake M. J. and Yaxley G. (1997) Prediction of siderophile element metal–silicate partition coefficients to 20 GPa and 2800 °C: the effect of pressure, temperature, fO_2 and silicate and metallic melt composition. *Phys. Earth Planet. Int.* **100**, 115–134.

Righter K., Sutton S. R., Newville M., Le L., Schwandt C. S., Uchida H., Lavina B. and Downs R. T. (2006) Oxidation state of vanadium in spinel and silicate melt: implications for planetary basalts and mantle melting. *Am. Mineral.* **91**, 1643–1656.

Righter K., Humayun M. and Danielson L. R. (2008a) Metal–silicate partitioning of palladium during core formation. *Nat. Geosci.* **1**, 321–324.

Righter K., Chesley J. T., Caiazza C. M., Gibson, Jr., E. K. and Ruiz J. (2008b) Re and Os concentrations in arc basalts: The roles of volatility and source region fO_2 variations. *Geochim. Cosmochim. Acta* **72**, 926–947.

Ringwood A. E. (1979) *Origin of the Earth and Moon*. Springer, New York.

Rubie D. C., Melosh H. J., Reid J. E., Liebske C. and Righter K. (2003) Mechanisms of metal–silicate equilibration in the terrestrial magma ocean. *Earth Planet. Sci. Lett.* **205**, 239–255.

Schmidt G., Spettel B., and Palme H. (2003) Arsenic and Sb abundances in the Earth's mantle. LPSC **XXXIV**. #1581.

Schmitt W., Palme H. and Wanke H. (1989) Experimental determination of metal/silicate partition coefficients for P, Co, Ni, Cu, Ga, Ge, Mo, W and some implications for the early evolution of the Earth. *Geochim. Cosmochim. Acta* **53**, 173–186.

Shannon R. D. (1976) Revised effective ionic radii and systematic studies of interatomic distances in halides and chalcogenides. *Acta Crystall.* **A32**, 751–767.

Sims K. W. W., Newsom H. E. and Gladney E. S. (1990) Chemical fractionation during formation of the Earth's core and continental crust: clues from As, Sb, W and Mo. In *The Origin of the Earth* (eds. H. E. Newsom and J. H. Jones). Oxford Univ. Press, New York, pp. 291–318.

Sundman B., Jansson B. and Andersson J.-O. (1985) The Thermo-Calc databank system. *Calphad* **9**, 153–199.

Suzuki T. and Akaogi M. (1995) Element partitioning between olivine and silicate melt under high pressure. *Phys. Chem. Mineral.* **22**, 411–418.

Swartzendruber L. J., Itkin V. P. and Alcock C. B. (1991) The Fe–Ni (Iron–nickel) system. *J. Phase Equilib.* **12**, 288–312.

Swindle T. D., Kring D. A., Burkland M. K., Hill D. H. and Boynton W. V. (1998) Noble gases, bulk chemistry, and petrography of olivine-rich achondrites Eagles Nest and LEW88763: comparison to brachinites. *Met. Planet. Sci.* **33**, 31–48.

Takeda Y., Ishiwata S. and Yazawa A. (1983) Distribution of minor elements between liquid copper and calcium ferrite slag. *Trans. Jpn. Inst. Metals* **24**, 518–524.

Toplis M. J. (2005) The thermodynamics of iron and magnesium partitioning between olivine and liquid: criteria for assessing and predicting equilibrium in natural and experimental systems. *Contrib. Mineral. Petrol.* **149**, 22–39.

Voisin L., Hino M. and Itagaki K. (2003) Phase relations and activities in the Fe–Ni–Sb and Fe–Ni–Sb systems at 1423 K. *Mater. Trans.* **44**, 1–5.

Wade J. and Wood B. J. (2005) Core formation and the oxidation state of the Earth. *Earth Planet. Sci. Lett.* **236**, 78–95.

Walker D., Norby L. and Jones J. H. (1993) Superheating effects on metal–silicate partitioning of siderophile elements. *Science* **262**, 1858–1861.

Walter M. J. and Thibault Y. (1995) Partitioning of tungsten and molybdenum between metallic liquid and silicate melt. *Science* **270**, 1186–1189.

Walter M. J., Newsom H., Ertel W. and Holzheid A. (2000) Siderophile elements in the Earth and Moon: metal/silicate partitioning and implications for core formation. See Canup & Righter 2000, pp. 265–290.

Wänke H. (1981) Constitution of terrestrial planets. *Phil. Trans. Roy. Soc. Lond. A* **393**, 287–302.

Wasson J. T. (1985) *Meteorites: Their Record of the Early*. W.H. Freeman & Co., New York, 267pp.

Witt-Eickschen G., Palme H., O'Neill H. St. C. and Allan C. (2007) The abundances of volatile trace elements in the earth's mantle: new evidence from analyses of mantle xenoliths. Lunar Planet. Sci. **XXXVIII**. #1536.

Wolf R. and Anders E. (1980) Moon and Earth: compositional differences inferred from siderophiles, volatiles, and alkalis in basalts. *Geochim. Cosmochim. Acta* **44**, 2111–2124.

Wolf R., Woodrow A. and Anders A. (1979) Lunar basalts and pristine highland rocks: comparison of siderophile and volatile elements. In Proceedings of the 10th Lunar Planetary Science Conference, pp. 2107–2130.

Wood B. J., Walter M. J. and Wade J. (2006) Accretion of the Earth and segregation of its core. *Nature* **441**, 825–833.

Wood B. J., Wade J. and Kilburn M. (2008) Core formation and the oxidation state of the Earth: additional constraints from Nb, V and Cr partitioning. *Geochim. Cosmochim. Acta* **72**, 1415–1426.

Yazawa A. (1980) Distribution of various elements between copper, matte, and slag. *Erzmetall* **33**, 377–382.

Yi W., Halliday A. N., Alt J. C., Lee D.-C., Rehkämper M., Garcia M. O. and Su Y. (2000) Cadmium, indium, tin, tellurium, and sulfur in oceanic basalts: implications for chalcophile element fractionation in the Earth. *J. Geophys. Res.* **105**(B8), 18927–18948.

Yi W., Halliday A. N., Lee D.-C. and Christensen J. N. (1995) Indium and tin in basalts, sulfides and the mantle. *Geochim. Cosmochim. Acta* **59**, 5081–5090.

Young R. W., Duffy J. A., Hassall G. J. and Xu Z. (1992) Use of optical basicity concept for determining phosphorus and sulphur slag–metal partitions. *Ironmak. & Steelmak.* **19**, 201–219.

Associate editor: Bjorn Mysen